

# Emergence and circulation coupling of moist layers over the tropical Atlantic

Marc Prange<sup>1</sup>, Bjorn Stevens<sup>2</sup>, and Stefan Alexander Buehler<sup>1</sup>

<sup>1</sup>Universität Hamburg

<sup>2</sup>Max Planck Institute for Meteorology

March 13, 2024

## Abstract

Mid-tropospheric elevated moist layers (EMLs) near the melting level have been found in various regional observational studies in the tropics. Recently, a preponderance of EMLs in the presence of aggregated convection was found in cloud resolving simulations of radiative convective equilibrium (RCE), highlighting a significant circulation coupling. Here, we present global monthly EML occurrence rates based on reanalysis, yielding a broader view on where and when EMLs occur in the real world. Over the Atlantic, EML occurrence follows an annual cycle that maximizes in summer, aligning with maximized ITCZ intensity and organisation. Resembling the results in RCE, the large-scale circulation over the Atlantic shifts from a deep overturning in January to a bottom-heavy circulation in July. While EMLs embedded in the July cross-equatorial Hadley cell are found to be sourced from the ITCZ, EMLs north of the ITCZ emerge from the strongly sheared zonal flow over West Africa.

# Emergence and circulation coupling of moist layers over the tropical Atlantic

Marc Prange<sup>1,2</sup>, Bjorn Stevens<sup>3</sup>, Stefan A. Buehler<sup>1</sup>

<sup>1</sup>Universität Hamburg, Meteorologisches Institut, Bundesstraße 55, 20146 Hamburg, Germany

<sup>2</sup>Program in Atmospheric and Oceanic Sciences, Princeton University, Princeton, NJ, USA

<sup>3</sup>Max Planck Institut für Meteorologie, Bundesstraße 53, 20146 Hamburg, Germany

## Key Points:

- Mid-tropospheric moist layers are ubiquitous around the tropical rain belts and their occurrence is subject to a strong seasonal cycle over the Atlantic.
- Moist layers are associated with a more bottom-heavy large-scale circulation, resembling RCE-based results.
- Moist layers south of the Atlantic summer ITCZ are detrained from the ITCZ while moist layers in the north are sourced from the west African monsoon system.

---

Corresponding author: Marc Prange, [mp1506@princeton.edu](mailto:mp1506@princeton.edu)

## Abstract

Mid-tropospheric elevated moist layers (EMLs) near the melting level have been found in various regional observational studies in the tropics. Recently, a preponderance of EMLs in the presence of aggregated convection was found in cloud resolving simulations of radiative convective equilibrium (RCE), highlighting a significant circulation coupling. Here, we present global monthly EML occurrence rates based on reanalysis, yielding a broader view on where and when EMLs occur in the real world. Over the Atlantic, EML occurrence follows an annual cycle that maximizes in summer, aligning with maximized ITCZ intensity and organisation. Resembling the results in RCE, the large-scale circulation over the Atlantic shifts from a deep overturning in January to a bottom-heavy circulation in July. While EMLs embedded in the July cross-equatorial Hadley cell are found to be sourced from the ITCZ, EMLs north of the ITCZ emerge from the strongly sheared zonal flow over West Africa.

## Plain Language Summary

In the vicinity of thunderstorms, the atmosphere is typically dry enabling the moist boundary layer top to radiatively cool efficiently. This yields subsidence and surface divergence that is thought to feed moist air near the surface into the thunderstorm, favoring convective aggregation. Recent idealized simulations have shown that more aggregated convection is associated with an enhanced outflow of moist air in the mid-troposphere that inhibits boundary layer cooling and drives an overturning circulation above the boundary layer. Here, we provide a first observational quantification of mid-tropospheric moist layer occurrence globally on an annual time-scale. We find a significant annual cycle over the Atlantic with a maximum in summer, aligning with peak convective activity and organisation of the Atlantic rainbelt. We show that the Atlantic overturning circulation becomes vertically constrained by the moist layers, similar to the idealized simulations. Moist layers embedded in the Atlantic Hadley circulation are likely sourced from convection within the Atlantic rainbelt, while moist layers over the northern sub-tropical Atlantic emerge from zonal wind shear within the West African monsoon system.

## 1 Introduction

The work of Pierrehumbert (1995) popularized the view of conceptually splitting up the tropical atmosphere into two columns entailing a moist convective region and a dry subsiding region (Miller, 1997; Larson et al., 1999; Kelly & Randall, 2001; Bellon et al., 2003). This view is useful for assessing the tropics in a framework of global radiative-convective equilibrium (RCE), with the dry regions acting as "radiator fins" to send excess energy to space that was obtained in the "furnace" regions of deep convection. Maintaining the picture of the tropics as a two-column model, Kelly and Randall (2001) stress how the intensity of the tropical circulation is crucially dependent on the vertical distribution of free tropospheric water vapor in the subsidence regions. Increased lower free tropospheric humidity enhances radiative cooling and therefore subsidence and local mass flux (see also Fig. 4 of Sokol & Hartmann, 2022), yielding enhanced circulation strength under constant subsidence area. This emphasizes the need for a profound understanding of the subtropical free tropospheric humidity structure to understand the general circulation.

A similar picture of a two-column tropical atmosphere is painted by studies of cloud-resolving simulations run in RCE configuration. Earlier studies that contrasted the equilibrium states between smaller and larger domains at spatial thresholds around 200 km found that convection aggregates on larger domains, yielding a drier free troposphere and a stronger large-scale circulation than non-aggregated convection that is present on smaller domains (Bretherton et al., 2005; C. J. Muller & Held, 2012). This is because at the large-scale, self-aggregation effects dominate aggregation-hostile effects of cold pools, yield-

64 ing a radiatively driven deep overturning circulation that dries out the subsiding free tro-  
 65 posphere, suppressing convection (Jeevanjee & Romps, 2013; C. Muller et al., 2022). While  
 66 these general characteristics of a coupling between circulation and humidity through ag-  
 67 gregation appear robust across a variety of studies using various cloud-resolving mod-  
 68 els (C. Muller & Bony, 2015; Wing et al., 2017), significant differences among models  
 69 remain in the vertical structure of humidity, clouds, and circulation (Wing et al., 2018).

70 Recently, Sokol and Hartmann (2022) point out such differences in the ensemble  
 71 of cloud-resolving RCE-MIP (RCE-model intercomparison project) simulations, high-  
 72 lighting a coupling of the congestus mode and convective aggregation. They find that  
 73 about half the models participating within RCE-MIP produce a mid-level circulation that  
 74 is driven by enhanced radiative cooling from moisture and cloudiness detrained around  
 75 0° C. Using a 2D cloud-resolving model they performed a small ensemble of RCE sim-  
 76 ulations within which they find a positive feedback between enhanced mid-level mois-  
 77 ture detrainment and convective aggregation. They argue that reduced upper tropospheric  
 78 moisture associated with more aggregated convection increases radiatively driven mid-  
 79 level moisture divergence, enhancing mid-level subsidence and circulation strength at the  
 80 expense of the deep overturning. This raises the question whether variations of the trop-  
 81 ical large-scale overturning circulation associated with variability in mid-level moisture  
 82 can also be observed in more realistic settings and whether enhanced mid-level moisture  
 83 really is sourced from the convection.

84 Schulz and Stevens (2018) were the first to look at observations of the tropical at-  
 85 mosphere through the lens of "moisture space", a commonly used technique in RCE stud-  
 86 ies to enable a low-dimensional view of large-scale circulations driving moisture conver-  
 87 gence and self-aggregation. Based on single point, but long-term measurements on Bar-  
 88 bados, their results confirmed previous RCE studies (Bretherton et al., 2005; Jeevanjee  
 89 & Romps, 2013; C. Muller & Bony, 2015) in how radiatively driven low-level circulations  
 90 condition the atmosphere for deep convection. However, due to the local nature of their  
 91 study, effects of enhanced mid-level moisture on the circulation and on convective ag-  
 92 gregation may have been missed. In fact, other observational studies over the Atlantic,  
 93 with less of a focus on circulation, have previously highlighted layers of increased mid-  
 94 tropospheric moisture over the tropical Atlantic (Johnson et al., 1996; Stevens, 2017; Gut-  
 95 leben, Groß, Wirth, Emde, & Mayer, 2019; Gutleben et al., 2020; Fildier et al., 2023).

96 Here, our approach to test the RCE-based results of Sokol and Hartmann (2022)  
 97 is to, in a first step, look for mid-tropospheric moist layers, which we refer to as elevated  
 98 moist layers (EMLs), throughout the tropics. We do so based on one year of ERA5 re-  
 99 analysis data, to which we apply a previously introduced EML identification method (Prange  
 100 et al., 2021). We then characterise the seasonal dependence of EML occurrence over dif-  
 101 ferent ocean basins (Sect. 3.1) and exploit the strong dependence found over the Atlantic  
 102 to examine whether the coupling between EML occurrence and the large-scale overturn-  
 103 ing circulation is similar to results from RCE (Sect 3.2). Finally, we characterise the spatio-  
 104 temporal structure of EMLs around the Atlantic summer ITCZ (inter-tropical conver-  
 105 gence zone) through a Hovmoller analysis and examine whether EMLs are actually sourced  
 106 from the ITCZ (Sect. 3.3).

## 107 2 Data and methods

### 108 2.1 Reanalysis data

109 We use ECMWF Reanalysis v5 (ERA5) atmospheric data for the year 2021 on 0.25°  
 110 horizontal resolution, 137 vertical levels and interpolated from hourly to 3-hourly inter-  
 111 vals (Hersbach et al., 2020). We choose ERA5 since it previously showed a good capa-  
 112 bility in capturing EMLs when collocated with in-situ soundings, superior to two hyper-

113 spectral satellite retrieval products (Prange et al., 2023). We only consider data within  
 114 30° S to 30° N.

## 115 2.2 Moist layer identification

116 Our analysis builds upon an identification method for EMLs that enables a quan-  
 117 titative definition of what we consider an EML. The method is slightly modified from  
 118 that proposed by Prange et al. (2021) where a vertically smooth reference profile is de-  
 119 fined for each water vapor profile of interest by fitting a second-order polynomial against  
 120 the profile of the logarithmic water vapor volume mixing ratio (VMR). Here, we adjusted  
 121 the method in two ways. Firstly, the fitted profile is forced to match the VMR at the  
 122 top of the mixed layer at around 950 hPa rather than at the surface to avoid a dry bias  
 123 in the lower free troposphere. Secondly, the reference profile is transformed into relative  
 124 humidity (RH) using the temperature and pressure profiles of the respective dataset. Pos-  
 125 itive humidity anomalies are then identified and characterised by means of strength, height  
 126 and thickness in RH rather than VMR, which has the benefit that EMLs from different  
 127 heights are more comparable.

128 We identify EMLs by applying thresholds with regard to the three EML charac-  
 129 terization metrics. The EML strength is defined by the maximum RH anomaly within  
 130 the layer. The layer is considered if EML strength exceeds 30 % of RH anomaly. The top  
 131 and bottom of the anomalous layer are defined as the levels where the RH anomaly re-  
 132 duces to < 10 %. The anomaly thickness is defined as the pressure difference between  
 133 the anomaly top and bottom. We only consider anomalies with thickness > 50 hPa and  
 134 < 400 hPa as EMLs to filter small fluctuations and vertically extended anomalies that  
 135 are rather a vertically constant bias than a layer. The EML height is defined as the RH  
 136 anomaly’s mean pressure, weighted by the anomalous RH at each level. We mainly con-  
 137 sider mid-tropospheric EMLs with altitudes between 500 to 700 hPa.

138 Fig. 1 showcases an example of a mid-tropospheric EML. In Fig. 1c the positive RH  
 139 anomaly against the fitted reference profile shaded in blue is characterized by a strength  
 140 of 57 %, a thickness of 145 hPa, and an altitude of 590 hPa. The EML is found in a pre-  
 141 dominantly easterly flow (Fig. 1a). The mid-tropospheric EML extends meridionally be-  
 142 tween around 18° N to 5° N where a deep convective cell is found in the meridional cross-  
 143 section of RH anomaly (Fig. 1b). The EML shows an increase in height with distance  
 144 from the deep convection, which is also found in the 316 K isentrope highlighted by the  
 145 black contour, supporting that the moisture may have detrained isentropically. However,  
 146 the meridional flow component that could be driven by convective detrainment is neg-  
 147 ligible compared to the strong easterly mean flow, indicating that the moist layer has  
 148 rather been advected with the easterlies. We elaborate on the emergence of EMLs over  
 149 the Atlantic in Sect. 3.3.

## 150 2.3 Moisture space

151 A commonly used technique to distinguish the major dynamical regimes of moist  
 152 convective regions and dry subsiding regions of the tropics is to sort data into bins of  
 153 a vertically integrated measure of moisture (Bretherton et al., 2005; Schulz & Stevens,  
 154 2018; Lang et al., 2021; Sokol & Hartmann, 2022). The advantage is that the dimension-  
 155 ality is reduced from three spatiotemporal dimensions ( $x, y, t$ ) to one dimension of mois-  
 156 ture. This avoids problems with spatio-temporal shifts of circulation features and en-  
 157 ables a simplified view at characteristics of the general circulation and humidity distri-  
 158 bution in the tropics.

159 Here, we define the moisture space by sorting the data into 50 bins of IWV (inte-  
 160 grated water vapor), with the bin-edges being defined by equi-distant percentiles of IWV  
 161 to assure an even distribution of datapoints across bins. In our analysis, we consider the

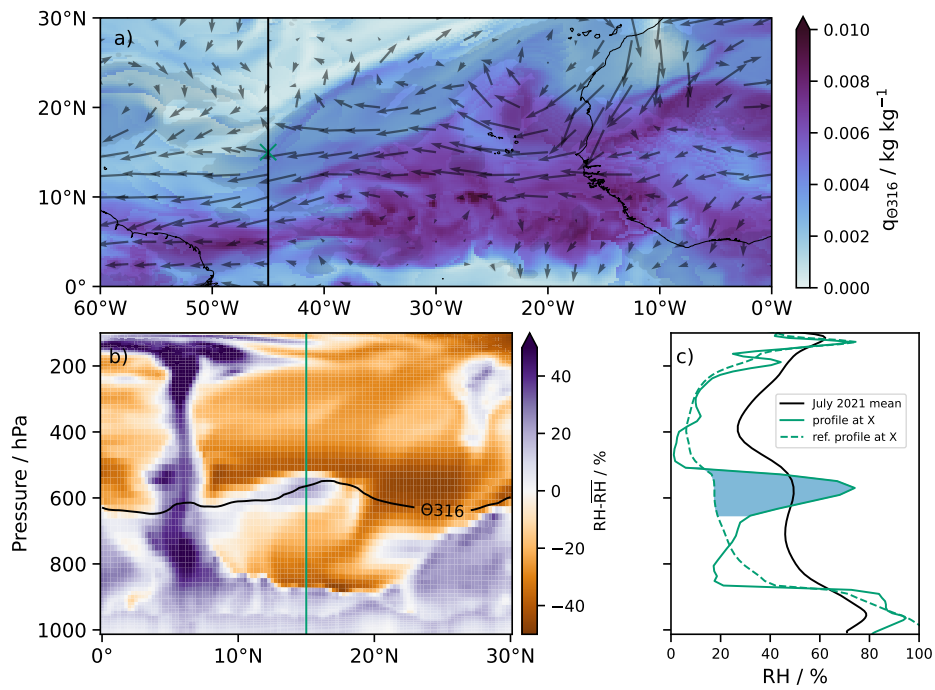


**Figure 1.** Overview of an EML case in ERA5 over the Northern Atlantic on July 19th, 2021 at 6 am UTC. a) shows mid-tropospheric specific humidity and flow along the 316 K isentrope. b) shows a meridional cross-section at  $45^\circ\text{W}$  (along black line in panel a) of RH anomaly with respect to the monthly mean. Black contour in b) highlights the 316 K isentrope. c) shows monthly mean RH profile in black, the instantaneous RH profile at  $15^\circ\text{N}$ ,  $45^\circ\text{W}$ , (green line b) ) and fitted reference profile used for identifying EML. Blue shaded area denotes identified RH anomaly that is characterized by anomaly strength, thickness, and height.

162 moisture space integrated over the Atlantic and for single months. In this case, every  
 163 bin in moisture space contains about 200,000 vertical profiles, which is plenty to obtain  
 164 robust statistics to an accuracy of 0.1 % RH (Lang et al., 2021). We quantify the circu-  
 165 lation in moisture space by means of the stream function  $\Psi(p)$  as defined by Sokol and  
 166 Hartmann (2022).

### 167 3 Results

#### 168 3.1 Global moist layer distribution and annual cycle

169 By applying our method for EML identification described in Sect. 2.2 to the ERA5  
 170 data and filtering only for mid-tropospheric EMLs between 500 to 700 hPa we obtain global  
 171 monthly distributions of EML occurrence rates for the year 2021 shown in Fig. 2. Over-  
 172 all, EML occurrence varies significantly in both zonal and meridional directions and over  
 173 the Atlantic also by season. In the west and east Pacific, seasonal variability is small,  
 174 but a persistent regional maximum in EML occurrence is found to the West of Peru. In  
 175 this usually dry region of persistent free-tropospheric subsidence the EMLs may signifi-  
 176 cantly alter the radiation budget, which can affect entrainment rates of low-level strato-  
 177 cumulus clouds (Stevens et al., 2003; Stevens & Brenguier, 2009). Maxima in EML oc-  
 178 currence are also found in regions around the precipitation bands, particularly around  
 179 the Atlantic ITCZ (inter-tropical convergence zone) in July.

180 We find relatively low EML occurrence rates within regions of high rainfall (red shad-  
 181 ing) such as the Western Pacific where moisture is known to be detrained from deep con-  
 182 vection near 0° C (Johnson et al., 1996). However, since RH is close to 80 % throughout  
 183 the column in these regions due to the ubiquity of deep convection (Johnson et al., 1999;  
 184 Romps, 2014), we do not identify this moisture as EMLs. This is desirable in our assess-  
 185 ment of EML-circulation coupling since detrained mid-level moisture embedded in a nearly  
 186 saturated atmospheric column does not have a strong effect on radiative cooling and hence  
 187 circulation (Pierrehumbert, 1998; Fildier et al., 2023).

188 To further study the interaction of EMLs and convection, we explore the seasonal  
 189 dependence of EMLs around the Atlantic ITCZ. In July, when the ITCZ shows the most  
 190 intense rainfall and organized convection (Biasutti et al., 2003; Hohenegger & Jakob, 2020),  
 191 EML occurrence is about double its value in January. This supports the idea of a cou-  
 192 pling between convective organization and mid-tropospheric moisture detrainment as sug-  
 193 gested by Sokol and Hartmann (2022). In the following, we examine whether this sea-  
 194 sonal dependence of EML occurrence over the Atlantic goes along with a change in the  
 195 overturning circulation that is consistent with RCE, or whether other moisture sources  
 196 are at play.

#### 197 3.2 Moist layer coupling to the large-scale circulation over the Atlantic

198 The annual cycle in EML occurrence over the tropical Atlantic is reflected in the  
 199 monthly mean RH structure depicted in moisture space in Fig. 3a and b. While the mid-  
 200 troposphere is mostly dry throughout the subsiding IWV regimes in January (i.e. IWV  
 201 percentile < 95), a secondary RH maximum emerges around 600 hPa in July that ex-  
 202 tends throughout subsiding moisture regimes. This feature is similar to some models in  
 203 the RCE-MIP comparison (e.g. UCLA-CRM and SAM-P3) shown by Sokol and Hart-  
 204 mann (2022). With the change to a more moist subsiding mid-troposphere in July we  
 205 also observe a shift from a deep overturning circulation in January (Fig. 3a) to a more  
 206 bottom-heavy circulation in July (Fig. 3b). The circulation in July is vertically constrained  
 207 by the height of the mid-tropospheric RH maximum where radiative cooling is enhanced,  
 208 consistent with the idea of a divergent moisture outflow feedback, as suggested by Sokol  
 209 and Hartmann (2022). To start addressing whether this concurrent shift of humidity struc-  
 210 ture and circulation through such a feedback is causal, we now shift our perspective from

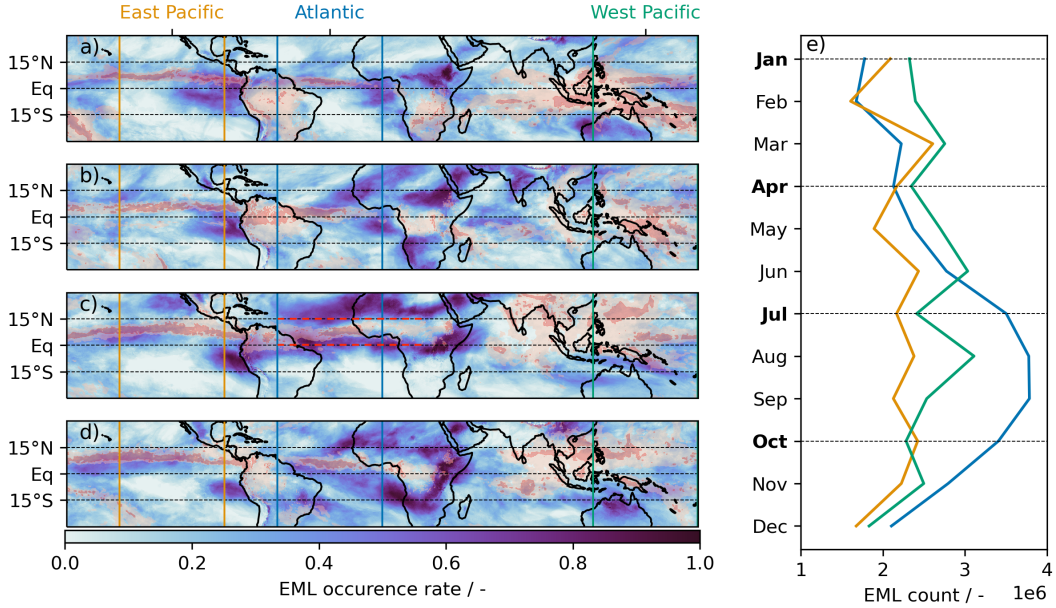


**Figure 2.** a) to d) show maps of monthly mid-tropospheric EML occurrence rates based on ERA5, i.e. the ratio of EMLs to the number of timesteps of the month. Maps are shown for January, April, July and October. Red contours on maps show 75th and 95th percentiles of rain rate to indicate convective activity. Red dashed lines on c) indicate cross-sections of Hovmöller diagrams in Fig. 4. EML occurrences are summed up over different ocean areas within 60°×60° longitude/latitude quadrants (land-filtered) and their annual evolution is shown panel e).

211 moisture space to zonal means to account for known meridional asymmetries of circula-  
 212 tion and humidity with respect to the deep convection that is mostly occurring within  
 213 the Atlantic ITCZ (Fig 3c-h).

214 On the zonal mean we observe the Hadley circulation (Fig. 3e+f), which in Janu-  
 215 ary and July is known to be dominated by a strong cross-equatorial Hadley cell with  
 216 its subsiding branch on the respective winter hemisphere (e.g. Peixoto, 1992; Trenberth  
 217 et al., 2000). This asymmetry in subsidence yields a more dry free troposphere on the  
 218 winter hemisphere, which is also reflected in the zonal means of IWV (Fig. 3c+d). The  
 219 circulations in moisture space (Fig. 3a+b) mostly reflect the respective cross-equatorial  
 220 Hadley cells since they are the main source of large-scale overturning over the Atlantic  
 221 (Peixoto, 1992). Hence, to explain the bottom-heaviness of the moisture space circula-  
 222 tion in July, we have to consider the moisture field within the July cross-equatorial Hadley  
 223 cell. Fig. 3h shows how in July EMLs occur abundantly North and South of the Atlantic  
 224 ITCZ, however, only the Southern ones are embedded within the Hadley cell and show  
 225 a direct circulation coupling through a mid-level circulation ( $-24 \text{ GTs}^{-1} \times 10$  isoline).  
 226 We conclude that the absence of EMLs north of the ITCZ in January allows for a deep  
 227 circulation in moisture space while the ubiquity of EMLs south of the ITCZ in July yields  
 228 a more bottom-heavy circulation.

### 229 3.3 Emergence of moist layers around the Atlantic summer ITCZ

230 We track mid-tropospheric EMLs around the Atlantic summer ITCZ through Hov-  
 231 möller diagrams by applying our method for EML identification (Sect. 2.2) along the zonal  
 232 cross-sections of the Atlantic and Africa between 60° W to 20° E at the equator (i.e. south  
 233 of the ITCZ, Fig. 4a) and at 15° N (i.e. north of the ITCZ, Fig. 4b) over the month of



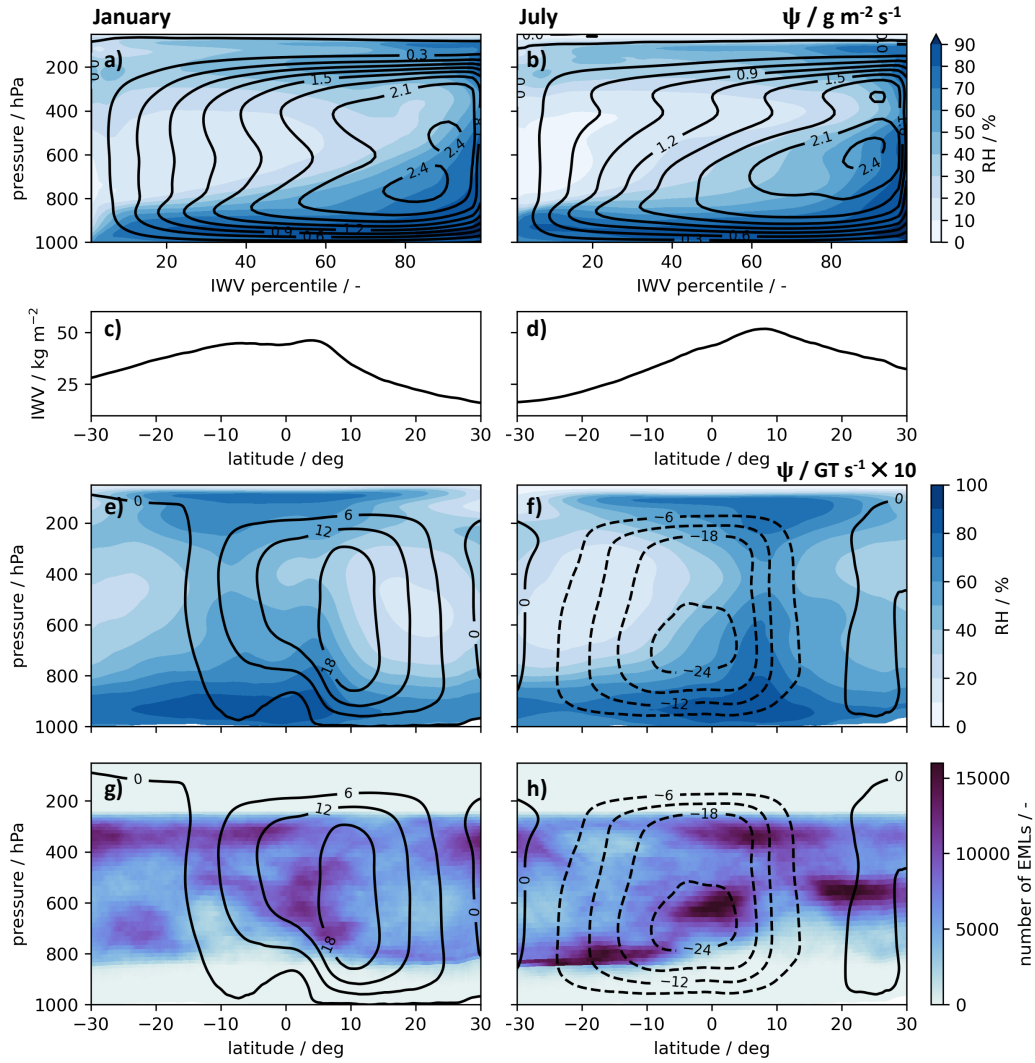


**Figure 3.** a) and b) show mean tropical Atlantic RH structure and circulation in terms of mass stream function  $\Psi$  in moisture space for January and July, respectively. c) to h) show zonal means over Atlantic ( $60^\circ \text{W}$  to  $0^\circ \text{W}$ ) of IWV, RH, stream function and number of EMLs for January (left) and July (right).

234 July 2021. The Hovmoller diagrams also indicate the direction of meridional wind through  
 235 hatched contours, revealing whether EMLs are embedded in southerly or northerly flow.  
 236 Having found that the EMLs at the equator are embedded within the cross-equatorial  
 237 Hadley cell (Fig. 3h) while the northern EMLs are not, we now examine at which spa-  
 238 tial and temporal scales EMLs emerge and live and whether the occurring EMLs coin-  
 239 cide with a meridional flow, that is indicative of the EML being detrained from the ITCZ.

240 The EMLs at the equator (Fig. 4) emerge and decay throughout the zonal cross-  
 241 section. EMLs are present in the east over the Gulf of Guinea and although they have  
 242 a slight easterly wind component they do not show a clear zonal propagation pattern across  
 243 the Atlantic. Instead, EMLs west of the Gulf of Guinea emerge over the open Atlantic  
 244 and generally within a northerly meridional wind. Particularly pronounced EMLs oc-  
 245 cur around July 22nd at  $30^\circ$  W and around July 27th at  $40^\circ$  W, lasting for around 3 to  
 246 4 days and showing a slight westward propagation. Overall, we find that 73% of EMLs  
 247 on the equatorial cross-section in July are embedded in a north-easterly flow, with a mean  
 248 u-wind of  $-4.9 \text{ m s}^{-1}$  and v-wind of  $-1.3 \text{ m s}^{-1}$ , indicating that the moisture is indeed sourced  
 249 from the ITCZ.

250 The pattern of EMLs and meridional winds on the  $15^\circ$  N Hovmoller diagram (Fig. 4b)  
 251 differs significantly from the equatorial one. EMLs mostly emerge around the West African  
 252 coastline near  $15^\circ$  W and are embedded in a stronger easterly flow with an average u-  
 253 wind of  $-11.6 \text{ m s}^{-1}$  within the EMLs and a more varying meridional wind that averages  
 254 to  $-0.8 \text{ m s}^{-1}$ . This underpins our conclusion from the zonal mean analysis (Fig. 3h) where  
 255 EMLs north of the ITCZ appear uncoupled to the Hadley circulation and instead sug-  
 256 gests that the dynamics over the West African continent are key for the emergence of  
 257 EMLs in the north with a strong easterly flow advecting them across the Atlantic.

258 In Fig. 4c we depict the July zonal mean cross-section from  $20^\circ$  W to the prime merid-  
 259 ian averaging over the West African continent and the Gulf of Guinea, highlighting some  
 260 main characteristics of the West African monsoon system (for a comprehensive review  
 261 consider Fink et al., 2017). Around  $10^\circ$  N lies the West African ITCZ denoted by high  
 262 RH throughout the troposphere, which is fed by a low-level south-westerly inflow of moist  
 263 Atlantic air in the monsoon layer (ML) coming in from the Gulf of Guinea (Marsham  
 264 et al., 2013). In addition, moisture is transported towards the ITCZ and the Sahel with  
 265 the Atlantic trade winds that deflect eastward around Senegal due to the West African  
 266 heat low (Lavaysse et al., 2009; Diekmann et al., 2021). This low-level moisture conver-  
 267 gence yields intense deep convection over West Africa at around  $10^\circ$  N, moistening the  
 268 entire column. This moistening coupled with a strongly sheared zonal mean flow from  
 269 westerlies in the ML to the African Easterly Jet (AEJ) in the mid-troposphere appears  
 270 as a prime producer of EMLs over the northern Atlantic in summer.

271 In addition, RH north of the West African ITCZ is enhanced near 500 hPa at the  
 272 top of the Saharan Air Layer (SAL). This is achieved through intense daytime adiabatic  
 273 mixing of low-level moist air that surges into the Saharan heat low from the south at night  
 274 and dry SAL air from aloft (Parker et al., 2005; Karam et al., 2008; Marsham et al., 2013).  
 275 Hence, particularly during daytime, enhanced RH and stratocumulus clouds are frequently  
 276 observed at the top of the SAL (Stein et al., 2011). Fig. 2c shows a preponderance of EMLs  
 277 over the Sahara, which could be explained through this mechanism. Again, the align-  
 278 ment of the enhanced mid-tropospheric moisture at the SAL top with the strongly sheared  
 279 zonal flow associated with the AEJ contributes to the production of EMLs over the north-  
 280 ern Atlantic in summer. A clear indication of EMLs originating from SAL airmasses is  
 281 that they were coherently found with increased mineral dust concentrations (Stevens,  
 282 2017; Gutleben, Groß, & Wirth, 2019)

283 Finally, we want to point out how the EMLs at  $15^\circ$  N are transported together with  
 284 patterns of alternating northerly and southerly meridional winds (Fig. 4b), which are in-  
 285 dicative of African Easterly Waves (AEWs) that form between May and October as dis-

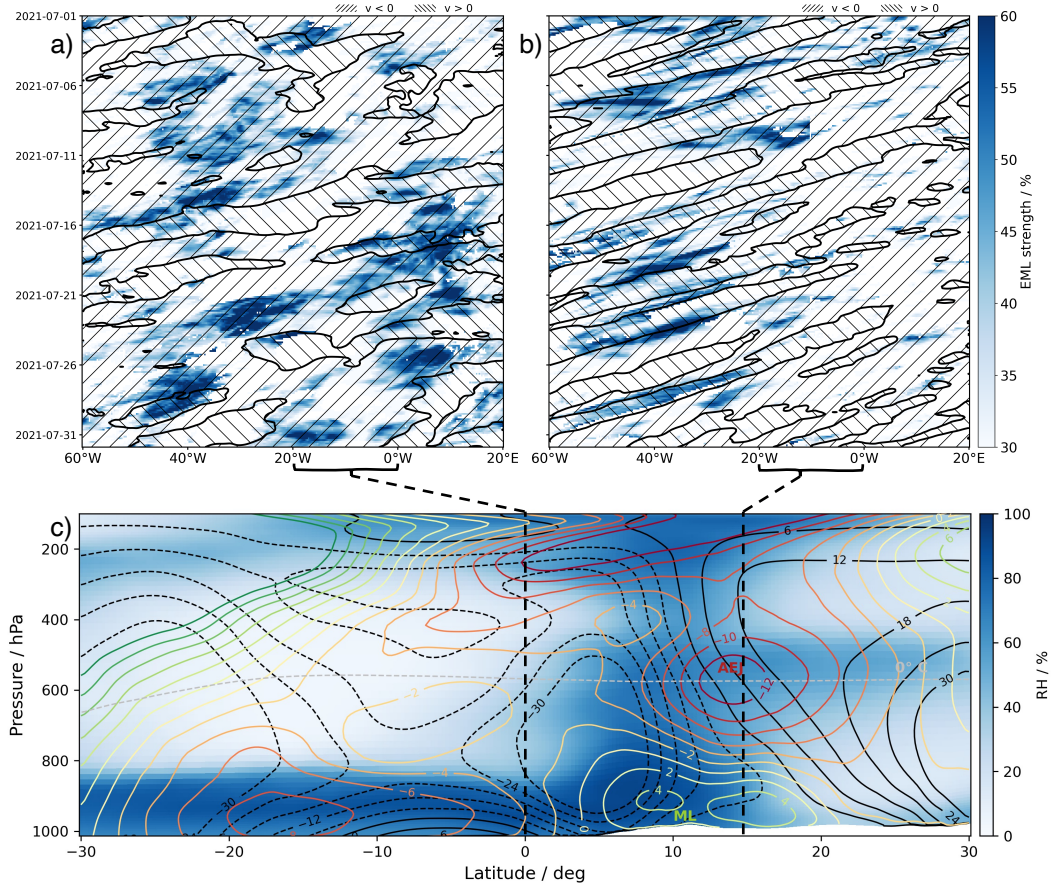


**Figure 4.** a) and b) show Hovmöller diagrams of EML strength and direction of meridional wind (hatched) averaged between 500 to 700 hPa along equator (a) and 15° N (b) between 60° W to 20° E (red dashed lines in Fig. 2c) for July 2021. Blue contours indicate the presence and strength of a mid-tropospheric EML. c) shows July zonal mean cross-section over West Africa and Gulf of Guinea (20° W to 0° W) of RH, stream function (black contours), zonal wind (red/green contours) and the 0° C isotherm (gray dashed contour). The positions of the African easterly jet (AEJ) and the monsoon layer (ML) are indicated.

286 turbances of the AEJ and act as predecessors of tropical cyclones (e.g. Thorncroft & Hodges,  
 287 2001; Kiladis et al., 2006; Mekonnen & Rossow, 2011). Enyew and Mekonnen (2021) high-  
 288 light how RH anomalies ahead of the AEW trough may favor the AEW’s development  
 289 into a tropical cyclone, indicating that EMLs may play a role in predicting AEW devel-  
 290 opment.

#### 291 4 Conclusion

292 We set out to look for layers of enhanced mid-tropospheric moisture (EMLs) through-  
 293 out the tropics based on one year of ERA5 data, motivated by a recently suggested cou-  
 294 pling of aggregated convection and a radiatively driven mid-level circulation in RCE (Sokol  
 295 & Hartmann, 2022). We find EML occurrence over the tropical Atlantic to have a pro-  
 296 nounced seasonal cycle, with a minimum in winter and a maximum in summer, allow-

297 ing us to test the RCE-based hypotheses about a moisture-circulation coupling in real-  
298 istic conditions.

299 The enhanced mid-level moisture over the Atlantic in July goes along with a shift  
300 to a more bottom-heavy circulation in moisture space when compared to the EML-sparse  
301 month January. However, we point out how meridional asymmetries in moisture and cir-  
302 culation around the convective regions can yield misleading deductions from moisture  
303 space alone. In particular, while EMLs occur north and south of the Atlantic summer  
304 ITCZ, only the southern ones are embedded within the cross-equatorial Hadley cell, cou-  
305 pling to the large-scale circulation. Since we find these EMLs to emerge throughout the  
306 Atlantic in a mostly northerly meridional flow from the ITCZ, we conclude that they are  
307 most likely sourced from deep convection within the ITCZ and indeed part of a radia-  
308 tively driven mid-level circulation as suggested by Sokol and Hartmann (2022).

309 While this moisture-circulation coupling resembles RCE-based results, here we only  
310 make a qualitative argument about how this can be explained by the degree of convec-  
311 tive aggregation and its ability to dry out the upper troposphere by referencing Hohenegger  
312 and Jakob (2020), who diagnose a more organised Atlantic ITCZ in boreal summer. Global  
313 storm resolving simulations may denote an interesting tool to more quantitatively ad-  
314 dress this since deep convective processes are resolved (Stevens et al., 2019).

315 North of the Atlantic summer ITCZ, EMLs are also ubiquitous but typically emerge  
316 over the West-African continent. The on average northerly meridional wind in these EMLs  
317 indicates no significant contribution of moisture detrained from the Atlantic ITCZ to the  
318 south. Instead, deep convection within the West-African ITCZ and vertical mixing of  
319 moist monsoonal air within the SAL moisten the West-African mid-troposphere, from  
320 where a sheared mean flow associated with the AEJ advects the moisture as EMLs across  
321 the Atlantic, along with AEWs. This result motivates further exploration of the coupling  
322 of EMLs and AEW development into tropical cyclones. In addition, the contributions  
323 of convective moisture sources compared to SAL mixing in producing EMLs over West  
324 Africa require further quantification. This may be addressed through further character-  
325 isation of EML dust loads as done for single cases by Gutleben, Groß, and Wirth (2019),  
326 e.g. from satellite observations or measurement campaigns. Another way to distinguish  
327 EML moisture sources is to calculate lagrangian backward trajectories, as done by Diekmann  
328 et al. (2021); Villiger et al. (2022), but specifically for a larger set of EML air parcels.

329 The results presented here may also have implications for constraining the clear-  
330 sky energy balance of CMIP (Climate Model Intercomparison Project) models. Recently,  
331 Feng et al. (2023) point out how biases in sub-tropical mid-tropospheric RH among CMIP6  
332 models yield a model spread of  $10 \text{ W m}^{-2}$  in clear-sky outgoing longwave radiation (OLR).  
333 This may be surprising at first given that most uncertainty in such models is typically  
334 associated with clouds (Stevens & Bony, 2013; Bony et al., 2015). However, it becomes  
335 perceivable when considering how large the spread of mid-tropospheric RH and circu-  
336 lation is in cloud-resolving RCE models as discussed by Sokol and Hartmann (2022). In  
337 addition, the added complexity of moisture sources and circulation coupling in more re-  
338 alistic settings discussed here might be difficult to capture by coarse models. Assessing  
339 EML characteristics of CMIP6 models with reference to the results presented here may  
340 help in narrowing down sources of mid-tropospheric RH biases between models and re-  
341 duce OLR biases.

## 342 Open Research Section

343 EML characteristics derived from ERA5 data is published on Zenodo, together with  
344 the analysis code (Prange et al., 2024).

## Acknowledgments

This research was funded by the Deutsche Forschungsgemeinschaft (DFG, German Research Foundation) under Germany’s Excellence Strategy—EXC 2037 “CLICCS—Climate, Climatic Change, and Society”—Project Number: 390683824, contribution to the Center for Earth System Research and Sustainability (CEN) of Universität Hamburg.

I thank Sandrine Bony for her initiating thoughts about a coupling to tropical waves and Nedjeljka Žagar for offering further insight on analysis methods of AEWs. I thank Lukas Klufft for technical assistance in wrangling with the data.

## References

- Bellon, G., Treut, H. L., & Ghil, M. (2003). Large-scale and evaporation-wind feedbacks in a box model of the tropical climate. *Geophysical Research Letters*, *30*(22). doi: 10.1029/2003gl017895
- Biasutti, M., Battisti, D. S., & Sarachik, E. S. (2003, August). The Annual Cycle over the Tropical Atlantic, South America, and Africa. *Journal of Climate*, *16*(15), 2491–2508. doi: 10.1175/1520-0442(2003)016<2491:TACOTT>2.0.CO;2
- Bony, S., Stevens, B., Frierson, D. M. W., Jakob, C., Kageyama, M., Pincus, R., ... Webb, M. J. (2015). Clouds, circulation and climate sensitivity. *Nature Geoscience*, *8*(4), 261–268. doi: 10.1038/ngeo2398
- Bretherton, C. S., Blossey, P. N., & Khairoutdinov, M. (2005). An Energy-Balance Analysis of Deep Convective Self-Aggregation above Uniform SST. *Journal of the Atmospheric Sciences*, *62*(12), 4273–4292. doi: 10.1175/jas3614.1
- Diekmann, C. J., Schneider, M., Knippertz, P., de Vries, A. J., Pfahl, S., Aemisegger, F., ... Braesicke, P. (2021). A Lagrangian Perspective on Stable Water Isotopes During the West African Monsoon. *Journal of Geophysical Research: Atmospheres*, *126*(19), e2021JD034895. doi: 10.1029/2021JD034895
- Enyew, B. D., & Mekonnen, A. (2021). The Interaction between African Easterly Waves and Different Types of Deep Convection and Its Influence on Atlantic Tropical Cyclones. *Atmosphere*, *13*(1), 5. doi: 10.3390/atmos13010005
- Feng, J., Paynter, D., Wang, C., & Menzel, R. (2023, September). How atmospheric humidity drives the outgoing longwave radiation–surface temperature relationship and inter-model spread. *Environmental Research Letters*, *18*(10), 104033. doi: 10.1088/1748-9326/acfb98
- Fildier, B., Muller, C., Pincus, R., & Fueglistaler, S. (2023). How Moisture Shapes Low-Level Radiative Cooling in Subsidence Regimes. *AGU Advances*, *4*(3). doi: 10.1029/2023av000880
- Fink, A. H., Engel, T., Ermert, V., van der Linden, R., Schneidewind, M., Redl, R., ... Janicot, S. (2017). Mean Climate and Seasonal Cycle. In *Meteorology of Tropical West Africa* (pp. 1–39). John Wiley & Sons, Ltd. doi: 10.1002/9781118391297.ch1
- Gutleben, M., Groß, S., & Wirth, M. (2019). Cloud macro-physical properties in Saharan-dust-laden and dust-free North Atlantic trade wind regimes: A lidar case study. *Atmospheric Chemistry and Physics*, *19*(16), 10659–10673. doi: 10.5194/acp-19-10659-2019
- Gutleben, M., Groß, S., Wirth, M., Emde, C., & Mayer, B. (2019). Impacts of Water Vapor on Saharan Air Layer Radiative Heating. *Geophysical Research Letters*, *46*(24), 14854–14862. doi: 10.1029/2019gl085344
- Gutleben, M., Groß, S., Wirth, M., & Mayer, B. (2020). Radiative effects of long-range-transported Saharan air layers as determined from airborne lidar measurements. *Atmospheric Chemistry and Physics*, *20*(20), 12313–12327. doi: 10.5194/acp-20-12313-2020
- Hersbach, H., Bell, B., Berrisford, P., Hirahara, S., Hořanyi, A., Muñoz-Sabater, J.,

- 397 ... Thépaut, J.-N. (2020). The ERA5 global reanalysis. *Quarterly Journal of*  
398 *the Royal Meteorological Society*, *146*(730), 1999–2049. doi: 10.1002/qj.3803
- 399 Hohenegger, C., & Jakob, C. (2020). A Relationship Between ITCZ Organi-  
400 zation and Subtropical Humidity. *Geophysical Research Letters*, *47*(16),  
401 e2020GL088515. doi: 10.1029/2020GL088515
- 402 Jeevanjee, N., & Romps, D. M. (2013). Convective self-aggregation, cold pools, and  
403 domain size. *Geophysical Research Letters*, *40*(5), 994–998. doi: 10.1002/grl  
404 .50204
- 405 Johnson, R. H., Ciesielski, P. E., & Hart, K. A. (1996, July). Tropical Inversions  
406 near the 0°C Level. *Journal of the Atmospheric Sciences*, *53*(13), 1838–1855.  
407 doi: 10.1175/1520-0469(1996)053(1838:TINTL)2.0.CO;2
- 408 Johnson, R. H., Rickenbach, T. M., Rutledge, S. A., Ciesielski, P. E., & Schubert,  
409 W. H. (1999). Trimodal Characteristics of Tropical Convection. *Journal of Cli-*  
410 *mate*, *12*(8), 2397–2418. doi: 10.1175/1520-0442(1999)012(2397:tcotc)2.0.co;2
- 411 Karam, D. B., Flamant, C., Knippertz, P., Reitebuch, O., Pelon, J., Chong, M.,  
412 & Dabas, A. (2008). Dust emissions over the Sahel associated with the  
413 West African monsoon intertropical discontinuity region: A representative  
414 case-study. *Quarterly Journal of the Royal Meteorological Society*, *134*(632),  
415 621–634. doi: 10.1002/qj.244
- 416 Kelly, M. A., & Randall, D. A. (2001). A Two-Box Model of a Zonal Atmospheric  
417 Circulation in the Tropics. *Journal of Climate*, *14*(19), 3944–3964. doi: 10  
418 .1175/1520-0442(2001)014(3944:atbmoa)2.0.co;2
- 419 Kiladis, G. N., Thorncroft, C. D., & Hall, N. M. J. (2006, September). Three-  
420 Dimensional Structure and Dynamics of African Easterly Waves. Part I:  
421 Observations. *Journal of the Atmospheric Sciences*, *63*(9), 2212–2230. doi:  
422 10.1175/JAS3741.1
- 423 Lang, T., Naumann, A. K., Stevens, B., & Buehler, S. A. (2021). Tropical Free-  
424 Tropospheric Humidity Differences and Their Effect on the Clear-Sky Ra-  
425 diation Budget in Global Storm-Resolving Models. *Journal of Advances in*  
426 *Modeling Earth Systems*, *13*(11). doi: 10.1029/2021ms002514
- 427 Larson, K., Hartmann, D. L., & Klein, S. A. (1999). The Role of Clouds, Wa-  
428 ter Vapor, Circulation, and Boundary Layer Structure in the Sensitiv-  
429 ity of the Tropical Climate. *Journal of Climate*, *12*(8), 2359–2374. doi:  
430 10.1175/1520-0442(1999)012
- 431 Lavaysse, C., Flamant, C., Janicot, S., Parker, D. J., Lafore, J.-P., Sultan, B., &  
432 Pelon, J. (2009, August). Seasonal evolution of the West African heat  
433 low: A climatological perspective. *Climate Dynamics*, *33*(2), 313–330. doi:  
434 10.1007/s00382-009-0553-4
- 435 Marsham, J. H., Dixon, N. S., Garcia-Carreras, L., Lister, G. M. S., Parker, D. J.,  
436 Knippertz, P., & Birch, C. E. (2013). The role of moist convection in the  
437 West African monsoon system: Insights from continental-scale convection-  
438 permitting simulations. *Geophysical Research Letters*, *40*(9), 1843–1849. doi:  
439 10.1002/grl.50347
- 440 Mekonnen, A., & Rossow, W. B. (2011). The Interaction Between Deep Convection  
441 and Easterly Waves over Tropical North Africa: A Weather State Perspective.  
442 *Journal of Climate*, *24*(16), 4276–4294. doi: 10.1175/2011jcli3900.1
- 443 Miller, R. L. (1997). Tropical Thermostats and Low Cloud Cover. *Journal of Cli-*  
444 *mate*, *10*(3), 409–440. doi: 10.1175/1520-0442(1997)010(0409:ttalcc)2.0.co;2
- 445 Muller, C., & Bony, S. (2015). What favors convective aggregation and why? *Geo-*  
446 *physical Research Letters*, *42*(13), 5626–5634. doi: 10.1002/2015gl064260
- 447 Muller, C., Yang, D., Craig, G., Cronin, T., Fildier, B., Haerter, J. O., ... Sher-  
448 wood, S. C. (2022). Spontaneous Aggregation of Convective Storms. *Annual*  
449 *Review of Fluid Mechanics*, *54*(1), 133–157. doi: 10.1146/annurev-fluid-022421  
450 -011319
- 451 Muller, C. J., & Held, I. M. (2012). Detailed Investigation of the Self-Aggregation

- of Convection in Cloud-Resolving Simulations. *Journal of the Atmospheric Sciences*, 69(8), 2551–2565. doi: 10.1175/jas-d-11-0257.1
- Parker, D. J., Thorncroft, C. D., Burton, R. R., & Diongue-Niang, A. (2005). Analysis of the African easterly jet, using aircraft observations from the JET2000 experiment. *Quarterly Journal of the Royal Meteorological Society*, 131(608), 1461–1482. doi: 10.1256/qj.03.189
- Peixoto, A. H. O., Jose P. (1992). *Physics of Climate* (1st ed.). American Institute of Physics Melville, NY.
- Pierrehumbert, R. T. (1995). Thermostats, Radiator Fins, and the Local Runaway Greenhouse. *Journal of the Atmospheric Sciences*, 52(10), 1784–1806. doi: 10.1175/1520-0469(1995)052
- Pierrehumbert, R. T. (1998). Lateral mixing as a source of subtropical water vapor. *Geophysical Research Letters*, 25(2), 151–154. doi: 10.1029/97GL03563
- Prange, M., Brath, M., & Buehler, S. A. (2021). Are elevated moist layers a blind spot for hyperspectral infrared sounders? A model study. *Atmospheric Measurement Techniques*, 14(11), 7025–7044. doi: 10.5194/amt-14-7025-2021
- Prange, M., Buehler, S. A., & Brath, M. (2023). How adequately are elevated moist layers represented in reanalysis and satellite observations? *Atmospheric Chemistry and Physics*, 23(1), 725–741. doi: 10.5194/acp-23-725-2023
- Prange, M., Stevens, B., & Buehler, S. A. (2024). *Supplementary data for "Emergence and circulation coupling of moist layers over the tropical Atlantic"*. Zenodo [Dataset, Software]. doi: 10.5281/zenodo.10667051
- Romps, D. M. (2014). An Analytical Model for Tropical Relative Humidity. *Journal of Climate*, 27(19), 7432–7449. doi: 10.1175/jcli-d-14-00255.1
- Schulz, H., & Stevens, B. (2018). Observing the Tropical Atmosphere in Moisture Space. *Journal of the Atmospheric Sciences*, 75(10), 3313–3330. doi: 10.1175/jas-d-17-0375.1
- Sokol, A. B., & Hartmann, D. L. (2022). Congestus Mode Invigoration by Convective Aggregation in Simulations of Radiative-Convective Equilibrium. *Journal of Advances in Modeling Earth Systems*, 14(7), e2022MS003045. doi: 10.1029/2022MS003045
- Stein, T. H. M., Parker, D. J., Delanoë, J., Dixon, N. S., Hogan, R. J., Knipertz, P., ... Marsham, J. H. (2011). The vertical cloud structure of the West African monsoon: A 4 year climatology using CloudSat and CALIPSO. *Journal of Geophysical Research: Atmospheres*, 116(D22). doi: 10.1029/2011JD016029
- Stevens, B. (2017, June). Clouds unfazed by haze. *Nature*, 546(7659), 483–484. doi: 10.1038/546483a
- Stevens, B., & Bony, S. (2013). What Are Climate Models Missing? *Science*, 340(6136), 1053–1054. doi: 10.1126/science.1237554
- Stevens, B., & Brenguier, J.-L. (2009, February). Cloud-controlling Factors: Low Clouds. In J. Heintzenberg & R. J. Charlson (Eds.), *Clouds in the Perturbed Climate System: Their Relationship to Energy Balance, Atmospheric Dynamics, and Precipitation* (p. 0). The MIT Press. doi: 10.7551/mitpress/9780262012874.003.0008
- Stevens, B., Lenschow, D. H., Faloona, I., Moeng, C.-H., Lilly, D. K., Blomquist, B., ... Thornton, D. (2003). On entrainment rates in nocturnal marine stratocumulus. *Quarterly Journal of the Royal Meteorological Society*, 129(595), 3469–3493. doi: 10.1256/qj.02.202
- Stevens, B., Satoh, M., Auger, L., Biercamp, J., Bretherton, C. S., Chen, X., ... Zhou, L. (2019). DYAMOND: The DYNAMics of the Atmospheric general circulation Modeled On Non-hydrostatic Domains. *Progress in Earth and Planetary Science*, 6(1), 61. doi: 10.1186/s40645-019-0304-z
- Thorncroft, C., & Hodges, K. (2001, March). African Easterly Wave Variability and Its Relationship to Atlantic Tropical Cyclone Activity. *Journal of Climate*,

- 507           14(6), 1166–1179. doi: 10.1175/1520-0442(2001)014(1166:AEWVAI)2.0.CO;2  
508   Trenberth, K. E., Stepaniak, D. P., & Caron, J. M. (2000, November). The Global  
509   Monsoon as Seen through the Divergent Atmospheric Circulation. *Journal of*  
510   *Climate*, 13(22), 3969–3993. doi: 10.1175/1520-0442(2000)013(3969:TGMAS)  
511   2.0.CO;2
- 512   Villiger, L., Wernli, H., Boettcher, M., Hagen, M., & Aemisegger, F. (2022). La-  
513   grangian formation pathways of moist anomalies in the trade-wind region dur-  
514   ing the dry season: Two case studies from EUREC4A. *Weather and Climate*  
515   *Dynamics*, 3(1), 59–88. doi: 10.5194/wcd-3-59-2022
- 516   Wing, A. A., Emanuel, K., Holloway, C. E., & Muller, C. (2017). Convective Self-  
517   Aggregation in Numerical Simulations: A Review. *Surveys in Geophysics*,  
518   38(6), 1173–1197. doi: 10.1007/s10712-017-9408-4
- 519   Wing, A. A., Reed, K. A., Satoh, M., Stevens, B., Bony, S., & Ohno, T. (2018).  
520   Radiative–convective equilibrium model intercomparison project. *Geoscientific*  
521   *Model Development*, 11(2), 793–813. doi: 10.5194/gmd-11-793-2018



# Emergence and circulation coupling of moist layers over the tropical Atlantic

Marc Prange<sup>1,2</sup>, Bjorn Stevens<sup>3</sup>, Stefan A. Buehler<sup>1</sup>

<sup>1</sup>Universität Hamburg, Meteorologisches Institut, Bundesstraße 55, 20146 Hamburg, Germany

<sup>2</sup>Program in Atmospheric and Oceanic Sciences, Princeton University, Princeton, NJ, USA

<sup>3</sup>Max Planck Institut für Meteorologie, Bundesstraße 53, 20146 Hamburg, Germany

## Key Points:

- Mid-tropospheric moist layers are ubiquitous around the tropical rain belts and their occurrence is subject to a strong seasonal cycle over the Atlantic.
- Moist layers are associated with a more bottom-heavy large-scale circulation, resembling RCE-based results.
- Moist layers south of the Atlantic summer ITCZ are detrained from the ITCZ while moist layers in the north are sourced from the west African monsoon system.

---

Corresponding author: Marc Prange, [mp1506@princeton.edu](mailto:mp1506@princeton.edu)

**Abstract**

Mid-tropospheric elevated moist layers (EMLs) near the melting level have been found in various regional observational studies in the tropics. Recently, a preponderance of EMLs in the presence of aggregated convection was found in cloud resolving simulations of radiative convective equilibrium (RCE), highlighting a significant circulation coupling. Here, we present global monthly EML occurrence rates based on reanalysis, yielding a broader view on where and when EMLs occur in the real world. Over the Atlantic, EML occurrence follows an annual cycle that maximizes in summer, aligning with maximized ITCZ intensity and organisation. Resembling the results in RCE, the large-scale circulation over the Atlantic shifts from a deep overturning in January to a bottom-heavy circulation in July. While EMLs embedded in the July cross-equatorial Hadley cell are found to be sourced from the ITCZ, EMLs north of the ITCZ emerge from the strongly sheared zonal flow over West Africa.

**Plain Language Summary**

In the vicinity of thunderstorms, the atmosphere is typically dry enabling the moist boundary layer top to radiatively cool efficiently. This yields subsidence and surface divergence that is thought to feed moist air near the surface into the thunderstorm, favoring convective aggregation. Recent idealized simulations have shown that more aggregated convection is associated with an enhanced outflow of moist air in the mid-troposphere that inhibits boundary layer cooling and drives an overturning circulation above the boundary layer. Here, we provide a first observational quantification of mid-tropospheric moist layer occurrence globally on an annual time-scale. We find a significant annual cycle over the Atlantic with a maximum in summer, aligning with peak convective activity and organisation of the Atlantic rainbelt. We show that the Atlantic overturning circulation becomes vertically constrained by the moist layers, similar to the idealized simulations. Moist layers embedded in the Atlantic Hadley circulation are likely sourced from convection within the Atlantic rainbelt, while moist layers over the northern sub-tropical Atlantic emerge from zonal wind shear within the West African monsoon system.

**1 Introduction**

The work of Pierrehumbert (1995) popularized the view of conceptually splitting up the tropical atmosphere into two columns entailing a moist convective region and a dry subsiding region (Miller, 1997; Larson et al., 1999; Kelly & Randall, 2001; Bellon et al., 2003). This view is useful for assessing the tropics in a framework of global radiative-convective equilibrium (RCE), with the dry regions acting as "radiator fins" to send excess energy to space that was obtained in the "furnace" regions of deep convection. Maintaining the picture of the tropics as a two-column model, Kelly and Randall (2001) stress how the intensity of the tropical circulation is crucially dependent on the vertical distribution of free tropospheric water vapor in the subsidence regions. Increased lower free tropospheric humidity enhances radiative cooling and therefore subsidence and local mass flux (see also Fig. 4 of Sokol & Hartmann, 2022), yielding enhanced circulation strength under constant subsidence area. This emphasizes the need for a profound understanding of the subtropical free tropospheric humidity structure to understand the general circulation.

A similar picture of a two-column tropical atmosphere is painted by studies of cloud-resolving simulations run in RCE configuration. Earlier studies that contrasted the equilibrium states between smaller and larger domains at spatial thresholds around 200 km found that convection aggregates on larger domains, yielding a drier free troposphere and a stronger large-scale circulation than non-aggregated convection that is present on smaller domains (Bretherton et al., 2005; C. J. Muller & Held, 2012). This is because at the large-scale, self-aggregation effects dominate aggregation-hostile effects of cold pools, yield-

64 ing a radiatively driven deep overturning circulation that dries out the subsiding free tro-  
65 posphere, suppressing convection (Jeevanjee & Romps, 2013; C. Muller et al., 2022). While  
66 these general characteristics of a coupling between circulation and humidity through ag-  
67 gregation appear robust across a variety of studies using various cloud-resolving mod-  
68 els (C. Muller & Bony, 2015; Wing et al., 2017), significant differences among models  
69 remain in the vertical structure of humidity, clouds, and circulation (Wing et al., 2018).

70 Recently, Sokol and Hartmann (2022) point out such differences in the ensemble  
71 of cloud-resolving RCE-MIP (RCE-model intercomparison project) simulations, high-  
72 lighting a coupling of the congestus mode and convective aggregation. They find that  
73 about half the models participating within RCE-MIP produce a mid-level circulation that  
74 is driven by enhanced radiative cooling from moisture and cloudiness detrained around  
75 0° C. Using a 2D cloud-resolving model they performed a small ensemble of RCE sim-  
76 ulations within which they find a positive feedback between enhanced mid-level mois-  
77 ture detrainment and convective aggregation. They argue that reduced upper tropospheric  
78 moisture associated with more aggregated convection increases radiatively driven mid-  
79 level moisture divergence, enhancing mid-level subsidence and circulation strength at the  
80 expense of the deep overturning. This raises the question whether variations of the trop-  
81 ical large-scale overturning circulation associated with variability in mid-level moisture  
82 can also be observed in more realistic settings and whether enhanced mid-level moisture  
83 really is sourced from the convection.

84 Schulz and Stevens (2018) were the first to look at observations of the tropical at-  
85 mosphere through the lens of "moisture space", a commonly used technique in RCE stud-  
86 ies to enable a low-dimensional view of large-scale circulations driving moisture conver-  
87 gence and self-aggregation. Based on single point, but long-term measurements on Bar-  
88 bados, their results confirmed previous RCE studies (Bretherton et al., 2005; Jeevanjee  
89 & Romps, 2013; C. Muller & Bony, 2015) in how radiatively driven low-level circulations  
90 condition the atmosphere for deep convection. However, due to the local nature of their  
91 study, effects of enhanced mid-level moisture on the circulation and on convective ag-  
92 gregation may have been missed. In fact, other observational studies over the Atlantic,  
93 with less of a focus on circulation, have previously highlighted layers of increased mid-  
94 tropospheric moisture over the tropical Atlantic (Johnson et al., 1996; Stevens, 2017; Gut-  
95 leben, Groß, Wirth, Emde, & Mayer, 2019; Gutleben et al., 2020; Fildier et al., 2023).

96 Here, our approach to test the RCE-based results of Sokol and Hartmann (2022)  
97 is to, in a first step, look for mid-tropospheric moist layers, which we refer to as elevated  
98 moist layers (EMLs), throughout the tropics. We do so based on one year of ERA5 re-  
99 analysis data, to which we apply a previously introduced EML identification method (Prange  
100 et al., 2021). We then characterise the seasonal dependence of EML occurrence over dif-  
101 ferent ocean basins (Sect. 3.1) and exploit the strong dependence found over the Atlantic  
102 to examine whether the coupling between EML occurrence and the large-scale overturn-  
103 ing circulation is similar to results from RCE (Sect 3.2). Finally, we characterise the spatio-  
104 temporal structure of EMLs around the Atlantic summer ITCZ (inter-tropical conver-  
105 gence zone) through a Hovmoller analysis and examine whether EMLs are actually sourced  
106 from the ITCZ (Sect. 3.3).

## 107 2 Data and methods

### 108 2.1 Reanalysis data

109 We use ECMWF Reanalysis v5 (ERA5) atmospheric data for the year 2021 on 0.25°  
110 horizontal resolution, 137 vertical levels and interpolated from hourly to 3-hourly inter-  
111 vals (Hersbach et al., 2020). We choose ERA5 since it previously showed a good capa-  
112 bility in capturing EMLs when collocated with in-situ soundings, superior to two hyper-

113 spectral satellite retrieval products (Prange et al., 2023). We only consider data within  
 114 30° S to 30° N.

## 115 2.2 Moist layer identification

116 Our analysis builds upon an identification method for EMLs that enables a quan-  
 117 titative definition of what we consider an EML. The method is slightly modified from  
 118 that proposed by Prange et al. (2021) where a vertically smooth reference profile is de-  
 119 fined for each water vapor profile of interest by fitting a second-order polynomial against  
 120 the profile of the logarithmic water vapor volume mixing ratio (VMR). Here, we adjusted  
 121 the method in two ways. Firstly, the fitted profile is forced to match the VMR at the  
 122 top of the mixed layer at around 950 hPa rather than at the surface to avoid a dry bias  
 123 in the lower free troposphere. Secondly, the reference profile is transformed into relative  
 124 humidity (RH) using the temperature and pressure profiles of the respective dataset. Pos-  
 125 itive humidity anomalies are then identified and characterised by means of strength, height  
 126 and thickness in RH rather than VMR, which has the benefit that EMLs from different  
 127 heights are more comparable.

128 We identify EMLs by applying thresholds with regard to the three EML charac-  
 129 terization metrics. The EML strength is defined by the maximum RH anomaly within  
 130 the layer. The layer is considered if EML strength exceeds 30 % of RH anomaly. The top  
 131 and bottom of the anomalous layer are defined as the levels where the RH anomaly re-  
 132 duces to < 10 %. The anomaly thickness is defined as the pressure difference between  
 133 the anomaly top and bottom. We only consider anomalies with thickness > 50 hPa and  
 134 < 400 hPa as EMLs to filter small fluctuations and vertically extended anomalies that  
 135 are rather a vertically constant bias than a layer. The EML height is defined as the RH  
 136 anomaly’s mean pressure, weighted by the anomalous RH at each level. We mainly con-  
 137 sider mid-tropospheric EMLs with altitudes between 500 to 700 hPa.

138 Fig. 1 showcases an example of a mid-tropospheric EML. In Fig. 1c the positive RH  
 139 anomaly against the fitted reference profile shaded in blue is characterized by a strength  
 140 of 57 %, a thickness of 145 hPa, and an altitude of 590 hPa. The EML is found in a pre-  
 141 dominantly easterly flow (Fig. 1a). The mid-tropospheric EML extends meridionally be-  
 142 tween around 18° N to 5° N where a deep convective cell is found in the meridional cross-  
 143 section of RH anomaly (Fig. 1b). The EML shows an increase in height with distance  
 144 from the deep convection, which is also found in the 316 K isentrope highlighted by the  
 145 black contour, supporting that the moisture may have detrained isentropically. However,  
 146 the meridional flow component that could be driven by convective detrainment is neg-  
 147 ligible compared to the strong easterly mean flow, indicating that the moist layer has  
 148 rather been advected with the easterlies. We elaborate on the emergence of EMLs over  
 149 the Atlantic in Sect. 3.3.

## 150 2.3 Moisture space

151 A commonly used technique to distinguish the major dynamical regimes of moist  
 152 convective regions and dry subsiding regions of the tropics is to sort data into bins of  
 153 a vertically integrated measure of moisture (Bretherton et al., 2005; Schulz & Stevens,  
 154 2018; Lang et al., 2021; Sokol & Hartmann, 2022). The advantage is that the dimension-  
 155 ality is reduced from three spatiotemporal dimensions ( $x, y, t$ ) to one dimension of mois-  
 156 ture. This avoids problems with spatio-temporal shifts of circulation features and en-  
 157 ables a simplified view at characteristics of the general circulation and humidity distri-  
 158 bution in the tropics.

159 Here, we define the moisture space by sorting the data into 50 bins of IWV (inte-  
 160 grated water vapor), with the bin-edges being defined by equi-distant percentiles of IWV  
 161 to assure an even distribution of datapoints across bins. In our analysis, we consider the

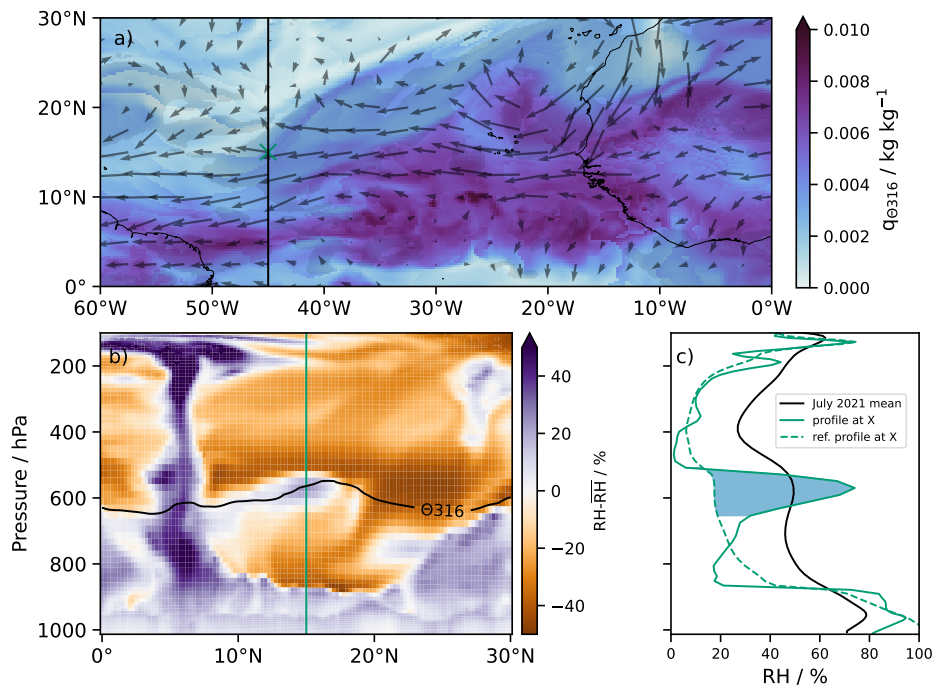


**Figure 1.** Overview of an EML case in ERA5 over the Northern Atlantic on July 19th, 2021 at 6 am UTC. a) shows mid-tropospheric specific humidity and flow along the 316 K isentrope. b) shows a meridional cross-section at  $45^\circ\text{W}$  (along black line in panel a) of RH anomaly with respect to the monthly mean. Black contour in b) highlights the 316 K isentrope. c) shows monthly mean RH profile in black, the instantaneous RH profile at  $15^\circ\text{N}$ ,  $45^\circ\text{W}$ , (green line b) ) and fitted reference profile used for identifying EML. Blue shaded area denotes identified RH anomaly that is characterized by anomaly strength, thickness, and height.

162 moisture space integrated over the Atlantic and for single months. In this case, every  
 163 bin in moisture space contains about 200,000 vertical profiles, which is plenty to obtain  
 164 robust statistics to an accuracy of 0.1 % RH (Lang et al., 2021). We quantify the circu-  
 165 lation in moisture space by means of the stream function  $\Psi(p)$  as defined by Sokol and  
 166 Hartmann (2022).

### 167 3 Results

#### 168 3.1 Global moist layer distribution and annual cycle

169 By applying our method for EML identification described in Sect. 2.2 to the ERA5  
 170 data and filtering only for mid-tropospheric EMLs between 500 to 700 hPa we obtain global  
 171 monthly distributions of EML occurrence rates for the year 2021 shown in Fig. 2. Over-  
 172 all, EML occurrence varies significantly in both zonal and meridional directions and over  
 173 the Atlantic also by season. In the west and east Pacific, seasonal variability is small,  
 174 but a persistent regional maximum in EML occurrence is found to the West of Peru. In  
 175 this usually dry region of persistent free-tropospheric subsidence the EMLs may signifi-  
 176 cantly alter the radiation budget, which can affect entrainment rates of low-level strato-  
 177 cumulus clouds (Stevens et al., 2003; Stevens & Brenguier, 2009). Maxima in EML oc-  
 178 currence are also found in regions around the precipitation bands, particularly around  
 179 the Atlantic ITCZ (inter-tropical convergence zone) in July.

180 We find relatively low EML occurrence rates within regions of high rainfall (red shad-  
 181 ing) such as the Western Pacific where moisture is known to be detrained from deep con-  
 182 vection near 0° C (Johnson et al., 1996). However, since RH is close to 80 % throughout  
 183 the column in these regions due to the ubiquity of deep convection (Johnson et al., 1999;  
 184 Romps, 2014), we do not identify this moisture as EMLs. This is desirable in our assess-  
 185 ment of EML-circulation coupling since detrained mid-level moisture embedded in a nearly  
 186 saturated atmospheric column does not have a strong effect on radiative cooling and hence  
 187 circulation (Pierrehumbert, 1998; Fildier et al., 2023).

188 To further study the interaction of EMLs and convection, we explore the seasonal  
 189 dependence of EMLs around the Atlantic ITCZ. In July, when the ITCZ shows the most  
 190 intense rainfall and organized convection (Biasutti et al., 2003; Hohenegger & Jakob, 2020),  
 191 EML occurrence is about double its value in January. This supports the idea of a cou-  
 192 pling between convective organization and mid-tropospheric moisture detrainment as sug-  
 193 gested by Sokol and Hartmann (2022). In the following, we examine whether this sea-  
 194 sonal dependence of EML occurrence over the Atlantic goes along with a change in the  
 195 overturning circulation that is consistent with RCE, or whether other moisture sources  
 196 are at play.

#### 197 3.2 Moist layer coupling to the large-scale circulation over the Atlantic

198 The annual cycle in EML occurrence over the tropical Atlantic is reflected in the  
 199 monthly mean RH structure depicted in moisture space in Fig. 3a and b. While the mid-  
 200 troposphere is mostly dry throughout the subsiding IWV regimes in January (i.e. IWV  
 201 percentile < 95), a secondary RH maximum emerges around 600 hPa in July that ex-  
 202 tends throughout subsiding moisture regimes. This feature is similar to some models in  
 203 the RCE-MIP comparison (e.g. UCLA-CRM and SAM-P3) shown by Sokol and Hart-  
 204 mann (2022). With the change to a more moist subsiding mid-troposphere in July we  
 205 also observe a shift from a deep overturning circulation in January (Fig. 3a) to a more  
 206 bottom-heavy circulation in July (Fig. 3b). The circulation in July is vertically constrained  
 207 by the height of the mid-tropospheric RH maximum where radiative cooling is enhanced,  
 208 consistent with the idea of a divergent moisture outflow feedback, as suggested by Sokol  
 209 and Hartmann (2022). To start addressing whether this concurrent shift of humidity struc-  
 210 ture and circulation through such a feedback is causal, we now shift our perspective from

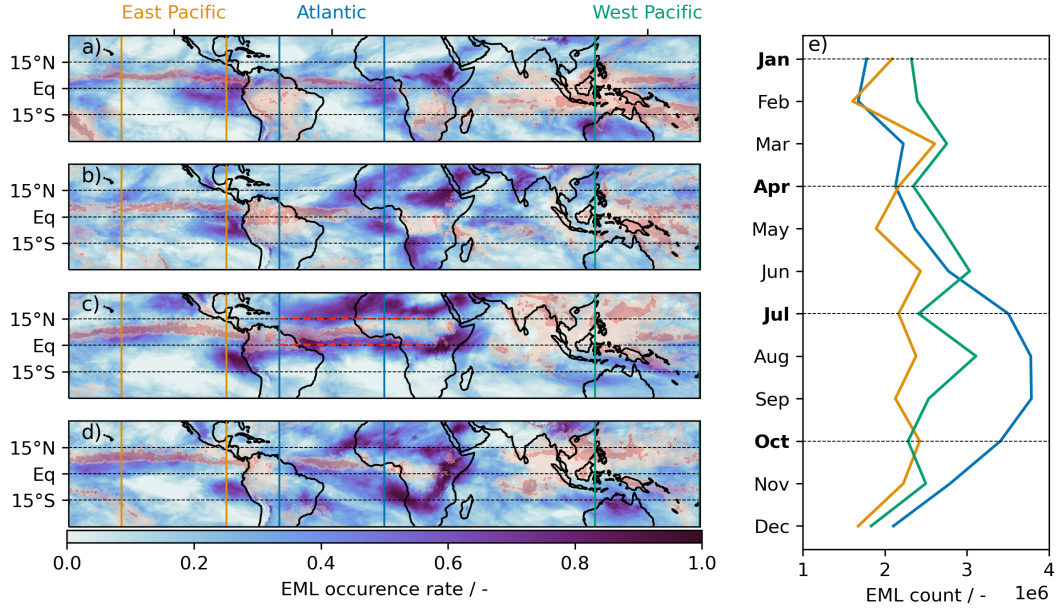


**Figure 2.** a) to d) show maps of monthly mid-tropospheric EML occurrence rates based on ERA5, i.e. the ratio of EMLs to the number of timesteps of the month. Maps are shown for January, April, July and October. Red contours on maps show 75th and 95th percentiles of rain rate to indicate convective activity. Red dashed lines on c) indicate cross-sections of Hovmöller diagrams in Fig. 4. EML occurrences are summed up over different ocean areas within 60°×60° longitude/latitude quadrants (land-filtered) and their annual evolution is shown panel e).

211 moisture space to zonal means to account for known meridional asymmetries of circula-  
 212 tion and humidity with respect to the deep convection that is mostly occurring within  
 213 the Atlantic ITCZ (Fig 3c-h).

214 On the zonal mean we observe the Hadley circulation (Fig. 3e+f), which in Janu-  
 215 ary and July is known to be dominated by a strong cross-equatorial Hadley cell with  
 216 its subsiding branch on the respective winter hemisphere (e.g. Peixoto, 1992; Trenberth  
 217 et al., 2000). This asymmetry in subsidence yields a more dry free troposphere on the  
 218 winter hemisphere, which is also reflected in the zonal means of IWV (Fig. 3c+d). The  
 219 circulations in moisture space (Fig. 3a+b) mostly reflect the respective cross-equatorial  
 220 Hadley cells since they are the main source of large-scale overturning over the Atlantic  
 221 (Peixoto, 1992). Hence, to explain the bottom-heaviness of the moisture space circula-  
 222 tion in July, we have to consider the moisture field within the July cross-equatorial Hadley  
 223 cell. Fig. 3h shows how in July EMLs occur abundantly North and South of the Atlantic  
 224 ITCZ, however, only the Southern ones are embedded within the Hadley cell and show  
 225 a direct circulation coupling through a mid-level circulation ( $-24 \text{ GTs}^{-1} \times 10$  isoline).  
 226 We conclude that the absence of EMLs north of the ITCZ in January allows for a deep  
 227 circulation in moisture space while the ubiquity of EMLs south of the ITCZ in July yields  
 228 a more bottom-heavy circulation.

### 229 3.3 Emergence of moist layers around the Atlantic summer ITCZ

230 We track mid-tropospheric EMLs around the Atlantic summer ITCZ through Hov-  
 231 möller diagrams by applying our method for EML identification (Sect. 2.2) along the zonal  
 232 cross-sections of the Atlantic and Africa between 60° W to 20° E at the equator (i.e. south  
 233 of the ITCZ, Fig. 4a) and at 15° N (i.e. north of the ITCZ, Fig. 4b) over the month of

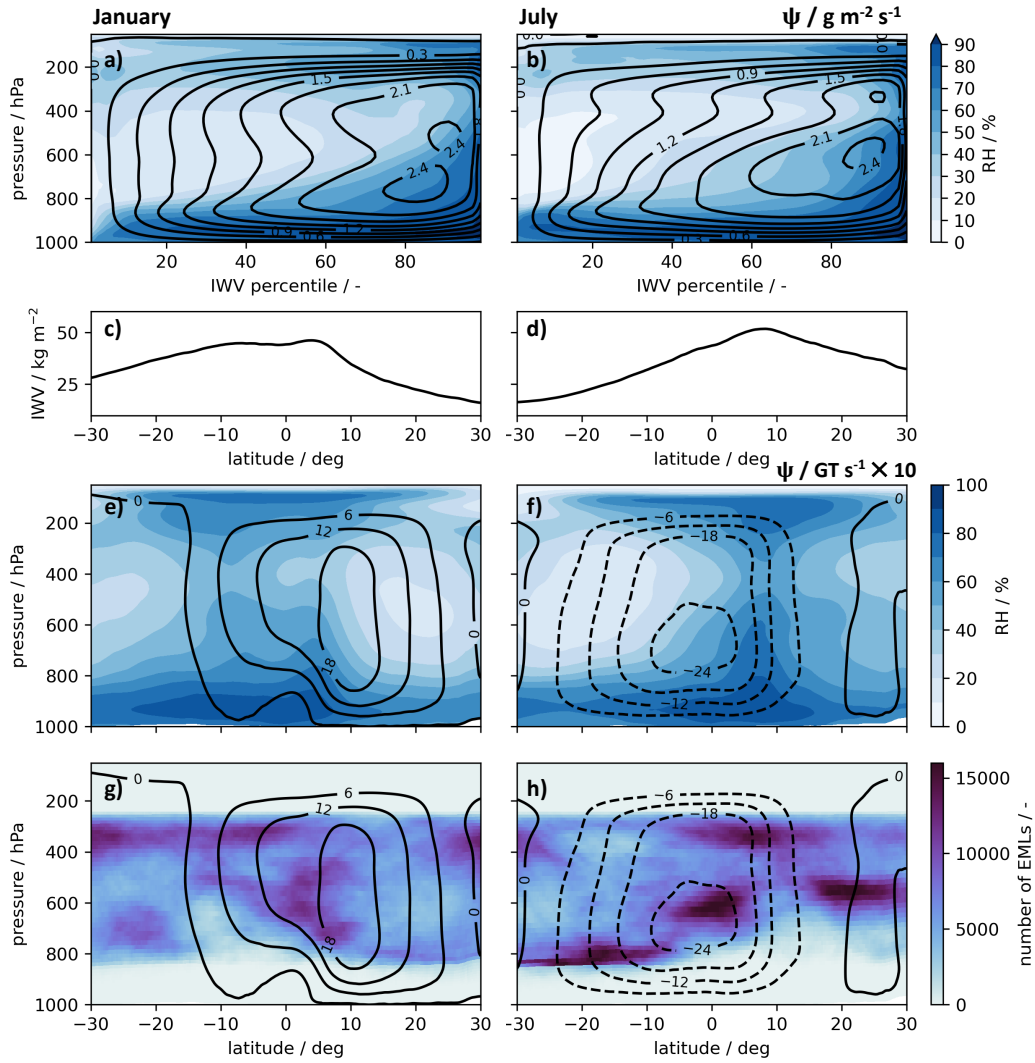


**Figure 3.** a) and b) show mean tropical Atlantic RH structure and circulation in terms of mass stream function  $\Psi$  in moisture space for January and July, respectively. c) to h) show zonal means over Atlantic (60° W to 0° W) of IWV, RH, stream function and number of EMLs for January (left) and July (right).



234 July 2021. The Hovmoller diagrams also indicate the direction of meridional wind through  
 235 hatched contours, revealing whether EMLs are embedded in southerly or northerly flow.  
 236 Having found that the EMLs at the equator are embedded within the cross-equatorial  
 237 Hadley cell (Fig. 3h) while the northern EMLs are not, we now examine at which spa-  
 238 tial and temporal scales EMLs emerge and live and whether the occurring EMLs coin-  
 239 cide with a meridional flow, that is indicative of the EML being detrained from the ITCZ.

240 The EMLs at the equator (Fig. 4) emerge and decay throughout the zonal cross-  
 241 section. EMLs are present in the east over the Gulf of Guinea and although they have  
 242 a slight easterly wind component they do not show a clear zonal propagation pattern across  
 243 the Atlantic. Instead, EMLs west of the Gulf of Guinea emerge over the open Atlantic  
 244 and generally within a northerly meridional wind. Particularly pronounced EMLs oc-  
 245 cur around July 22nd at 30° W and around July 27th at 40° W, lasting for around 3 to  
 246 4 days and showing a slight westward propagation. Overall, we find that 73% of EMLs  
 247 on the equatorial cross-section in July are embedded in a north-easterly flow, with a mean  
 248 u-wind of  $-4.9 \text{ m s}^{-1}$  and v-wind of  $-1.3 \text{ m s}^{-1}$ , indicating that the moisture is indeed sourced  
 249 from the ITCZ.

250 The pattern of EMLs and meridional winds on the 15° N Hovmoller diagram (Fig. 4b)  
 251 differs significantly from the equatorial one. EMLs mostly emerge around the West African  
 252 coastline near 15° W and are embedded in a stronger easterly flow with an average u-  
 253 wind of  $-11.6 \text{ m s}^{-1}$  within the EMLs and a more varying meridional wind that averages  
 254 to  $-0.8 \text{ m s}^{-1}$ . This underpins our conclusion from the zonal mean analysis (Fig. 3h) where  
 255 EMLs north of the ITCZ appear uncoupled to the Hadley circulation and instead sug-  
 256 gests that the dynamics over the West African continent are key for the emergence of  
 257 EMLs in the north with a strong easterly flow advecting them across the Atlantic.

258 In Fig. 4c we depict the July zonal mean cross-section from 20° W to the prime merid-  
 259 ian averaging over the West African continent and the Gulf of Guinea, highlighting some  
 260 main characteristics of the West African monsoon system (for a comprehensive review  
 261 consider Fink et al., 2017). Around 10° N lies the West African ITCZ denoted by high  
 262 RH throughout the troposphere, which is fed by a low-level south-westerly inflow of moist  
 263 Atlantic air in the monsoon layer (ML) coming in from the Gulf of Guinea (Marsham  
 264 et al., 2013). In addition, moisture is transported towards the ITCZ and the Sahel with  
 265 the Atlantic trade winds that deflect eastward around Senegal due to the West African  
 266 heat low (Lavaysse et al., 2009; Diekmann et al., 2021). This low-level moisture conver-  
 267 gence yields intense deep convection over West Africa at around 10° N, moistening the  
 268 entire column. This moistening coupled with a strongly sheared zonal mean flow from  
 269 westerlies in the ML to the African Easterly Jet (AEJ) in the mid-troposphere appears  
 270 as a prime producer of EMLs over the northern Atlantic in summer.

271 In addition, RH north of the West African ITCZ is enhanced near 500 hPa at the  
 272 top of the Saharan Air Layer (SAL). This is achieved through intense daytime adiabatic  
 273 mixing of low-level moist air that surges into the Saharan heat low from the south at night  
 274 and dry SAL air from aloft (Parker et al., 2005; Karam et al., 2008; Marsham et al., 2013).  
 275 Hence, particularly during daytime, enhanced RH and stratocumulus clouds are frequently  
 276 observed at the top of the SAL (Stein et al., 2011). Fig. 2c shows a preponderance of EMLs  
 277 over the Sahara, which could be explained through this mechanism. Again, the align-  
 278 ment of the enhanced mid-tropospheric moisture at the SAL top with the strongly sheared  
 279 zonal flow associated with the AEJ contributes to the production of EMLs over the north-  
 280 ern Atlantic in summer. A clear indication of EMLs originating from SAL airmasses is  
 281 that they were coherently found with increased mineral dust concentrations (Stevens,  
 282 2017; Gutleben, Groß, & Wirth, 2019)

283 Finally, we want to point out how the EMLs at 15° N are transported together with  
 284 patterns of alternating northerly and southerly meridional winds (Fig. 4b), which are in-  
 285 dicative of African Easterly Waves (AEWs) that form between May and October as dis-

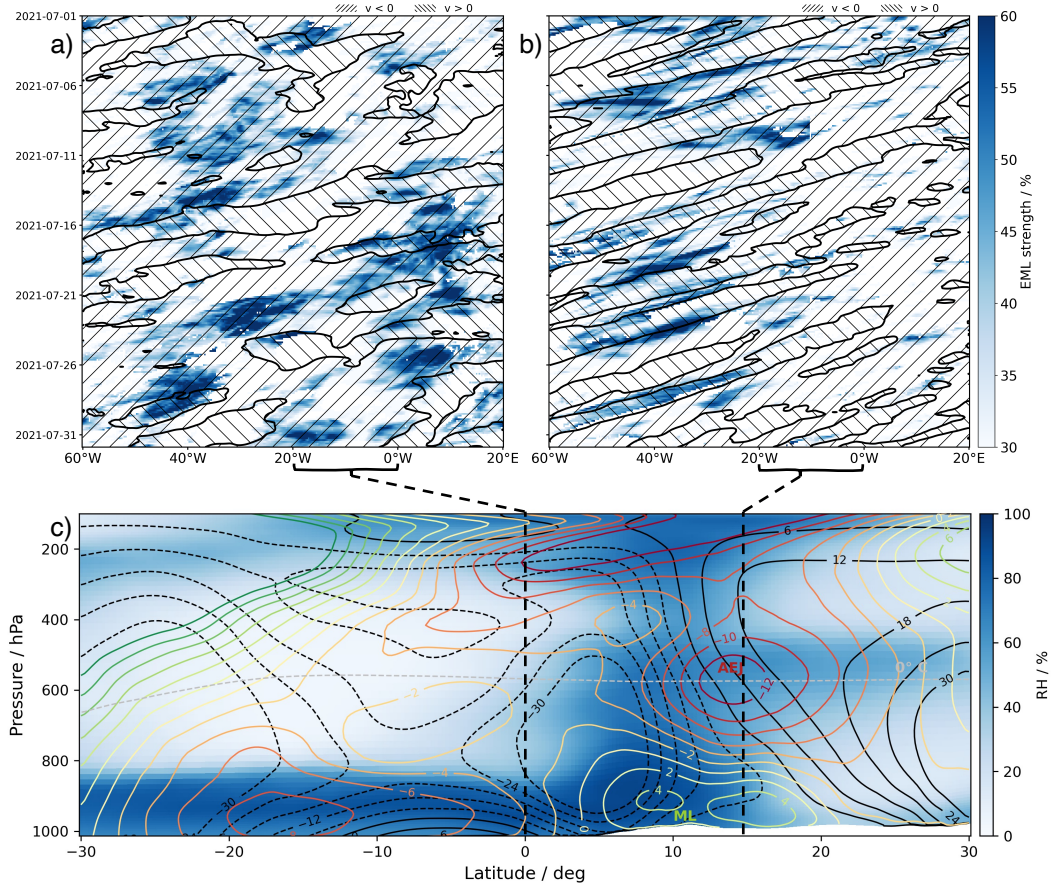


**Figure 4.** a) and b) show Hovmöller diagrams of EML strength and direction of meridional wind (hatched) averaged between 500 to 700 hPa along equator (a) and 15° N (b) between 60° W to 20° E (red dashed lines in Fig. 2c) for July 2021. Blue contours indicate the presence and strength of a mid-tropospheric EML. c) shows July zonal mean cross-section over West Africa and Gulf of Guinea (20° W to 0° W) of RH, stream function (black contours), zonal wind (red/green contours) and the 0° C isotherm (gray dashed contour). The positions of the African easterly jet (AEJ) and the monsoon layer (ML) are indicated.

286 turbances of the AEJ and act as predecessors of tropical cyclones (e.g. Thorncroft & Hodges,  
 287 2001; Kiladis et al., 2006; Mekonnen & Rossow, 2011). Enyew and Mekonnen (2021) high-  
 288 light how RH anomalies ahead of the AEW trough may favor the AEW’s development  
 289 into a tropical cyclone, indicating that EMLs may play a role in predicting AEW devel-  
 290 opment.

#### 291 4 Conclusion

292 We set out to look for layers of enhanced mid-tropospheric moisture (EMLs) through-  
 293 out the tropics based on one year of ERA5 data, motivated by a recently suggested cou-  
 294 pling of aggregated convection and a radiatively driven mid-level circulation in RCE (Sokol  
 295 & Hartmann, 2022). We find EML occurrence over the tropical Atlantic to have a pro-  
 296 nounced seasonal cycle, with a minimum in winter and a maximum in summer, allow-

297 ing us to test the RCE-based hypotheses about a moisture-circulation coupling in real-  
298 istic conditions.

299 The enhanced mid-level moisture over the Atlantic in July goes along with a shift  
300 to a more bottom-heavy circulation in moisture space when compared to the EML-sparse  
301 month January. However, we point out how meridional asymmetries in moisture and cir-  
302 culation around the convective regions can yield misleading deductions from moisture  
303 space alone. In particular, while EMLs occur north and south of the Atlantic summer  
304 ITCZ, only the southern ones are embedded within the cross-equatorial Hadley cell, cou-  
305 pling to the large-scale circulation. Since we find these EMLs to emerge throughout the  
306 Atlantic in a mostly northerly meridional flow from the ITCZ, we conclude that they are  
307 most likely sourced from deep convection within the ITCZ and indeed part of a radia-  
308 tively driven mid-level circulation as suggested by Sokol and Hartmann (2022).

309 While this moisture-circulation coupling resembles RCE-based results, here we only  
310 make a qualitative argument about how this can be explained by the degree of convec-  
311 tive aggregation and its ability to dry out the upper troposphere by referencing Hohenegger  
312 and Jakob (2020), who diagnose a more organised Atlantic ITCZ in boreal summer. Global  
313 storm resolving simulations may denote an interesting tool to more quantitatively ad-  
314 dress this since deep convective processes are resolved (Stevens et al., 2019).

315 North of the Atlantic summer ITCZ, EMLs are also ubiquitous but typically emerge  
316 over the West-African continent. The on average northerly meridional wind in these EMLs  
317 indicates no significant contribution of moisture detrained from the Atlantic ITCZ to the  
318 south. Instead, deep convection within the West-African ITCZ and vertical mixing of  
319 moist monsoonal air within the SAL moisten the West-African mid-troposphere, from  
320 where a sheared mean flow associated with the AEJ advects the moisture as EMLs across  
321 the Atlantic, along with AEWs. This result motivates further exploration of the coupling  
322 of EMLs and AEW development into tropical cyclones. In addition, the contributions  
323 of convective moisture sources compared to SAL mixing in producing EMLs over West  
324 Africa require further quantification. This may be addressed through further character-  
325 isation of EML dust loads as done for single cases by Gutleben, Groß, and Wirth (2019),  
326 e.g. from satellite observations or measurement campaigns. Another way to distinguish  
327 EML moisture sources is to calculate lagrangian backward trajectories, as done by Diekmann  
328 et al. (2021); Villiger et al. (2022), but specifically for a larger set of EML air parcels.

329 The results presented here may also have implications for constraining the clear-  
330 sky energy balance of CMIP (Climate Model Intercomparison Project) models. Recently,  
331 Feng et al. (2023) point out how biases in sub-tropical mid-tropospheric RH among CMIP6  
332 models yield a model spread of  $10 \text{ W m}^{-2}$  in clear-sky outgoing longwave radiation (OLR).  
333 This may be surprising at first given that most uncertainty in such models is typically  
334 associated with clouds (Stevens & Bony, 2013; Bony et al., 2015). However, it becomes  
335 perceivable when considering how large the spread of mid-tropospheric RH and circu-  
336 lation is in cloud-resolving RCE models as discussed by Sokol and Hartmann (2022). In  
337 addition, the added complexity of moisture sources and circulation coupling in more re-  
338 alistic settings discussed here might be difficult to capture by coarse models. Assessing  
339 EML characteristics of CMIP6 models with reference to the results presented here may  
340 help in narrowing down sources of mid-tropospheric RH biases between models and re-  
341 duce OLR biases.

## 342 Open Research Section

343 EML characteristics derived from ERA5 data is published on Zenodo, together with  
344 the analysis code (Prange et al., 2024).

## Acknowledgments

This research was funded by the Deutsche Forschungsgemeinschaft (DFG, German Research Foundation) under Germany’s Excellence Strategy—EXC 2037 “CLICCS—Climate, Climatic Change, and Society”—Project Number: 390683824, contribution to the Center for Earth System Research and Sustainability (CEN) of Universität Hamburg.

I thank Sandrine Bony for her initiating thoughts about a coupling to tropical waves and Nedjeljka Žagar for offering further insight on analysis methods of AEWs. I thank Lukas Klufft for technical assistance in wrangling with the data.

## References

- Bellon, G., Treut, H. L., & Ghil, M. (2003). Large-scale and evaporation-wind feedbacks in a box model of the tropical climate. *Geophysical Research Letters*, *30*(22). doi: 10.1029/2003gl017895
- Biasutti, M., Battisti, D. S., & Sarachik, E. S. (2003, August). The Annual Cycle over the Tropical Atlantic, South America, and Africa. *Journal of Climate*, *16*(15), 2491–2508. doi: 10.1175/1520-0442(2003)016<2491:TACOTT>2.0.CO;2
- Bony, S., Stevens, B., Frierson, D. M. W., Jakob, C., Kageyama, M., Pincus, R., ... Webb, M. J. (2015). Clouds, circulation and climate sensitivity. *Nature Geoscience*, *8*(4), 261–268. doi: 10.1038/ngeo2398
- Bretherton, C. S., Blossey, P. N., & Khairoutdinov, M. (2005). An Energy-Balance Analysis of Deep Convective Self-Aggregation above Uniform SST. *Journal of the Atmospheric Sciences*, *62*(12), 4273–4292. doi: 10.1175/jas3614.1
- Diekmann, C. J., Schneider, M., Knippertz, P., de Vries, A. J., Pfahl, S., Aemisegger, F., ... Braesicke, P. (2021). A Lagrangian Perspective on Stable Water Isotopes During the West African Monsoon. *Journal of Geophysical Research: Atmospheres*, *126*(19), e2021JD034895. doi: 10.1029/2021JD034895
- Enyew, B. D., & Mekonnen, A. (2021). The Interaction between African Easterly Waves and Different Types of Deep Convection and Its Influence on Atlantic Tropical Cyclones. *Atmosphere*, *13*(1), 5. doi: 10.3390/atmos13010005
- Feng, J., Paynter, D., Wang, C., & Menzel, R. (2023, September). How atmospheric humidity drives the outgoing longwave radiation–surface temperature relationship and inter-model spread. *Environmental Research Letters*, *18*(10), 104033. doi: 10.1088/1748-9326/acfb98
- Fildier, B., Muller, C., Pincus, R., & Fueglistaler, S. (2023). How Moisture Shapes Low-Level Radiative Cooling in Subsidence Regimes. *AGU Advances*, *4*(3). doi: 10.1029/2023av000880
- Fink, A. H., Engel, T., Ermert, V., van der Linden, R., Schneidewind, M., Redl, R., ... Janicot, S. (2017). Mean Climate and Seasonal Cycle. In *Meteorology of Tropical West Africa* (pp. 1–39). John Wiley & Sons, Ltd. doi: 10.1002/9781118391297.ch1
- Gutleben, M., Groß, S., & Wirth, M. (2019). Cloud macro-physical properties in Saharan-dust-laden and dust-free North Atlantic trade wind regimes: A lidar case study. *Atmospheric Chemistry and Physics*, *19*(16), 10659–10673. doi: 10.5194/acp-19-10659-2019
- Gutleben, M., Groß, S., Wirth, M., Emde, C., & Mayer, B. (2019). Impacts of Water Vapor on Saharan Air Layer Radiative Heating. *Geophysical Research Letters*, *46*(24), 14854–14862. doi: 10.1029/2019gl085344
- Gutleben, M., Groß, S., Wirth, M., & Mayer, B. (2020). Radiative effects of long-range-transported Saharan air layers as determined from airborne lidar measurements. *Atmospheric Chemistry and Physics*, *20*(20), 12313–12327. doi: 10.5194/acp-20-12313-2020
- Hersbach, H., Bell, B., Berrisford, P., Hirahara, S., Hořanyi, A., Muñoz-Sabater, J.,

- 397 ... Thépaut, J.-N. (2020). The ERA5 global reanalysis. *Quarterly Journal of*  
398 *the Royal Meteorological Society*, *146*(730), 1999–2049. doi: 10.1002/qj.3803
- 399 Hohenegger, C., & Jakob, C. (2020). A Relationship Between ITCZ Organi-  
400 zation and Subtropical Humidity. *Geophysical Research Letters*, *47*(16),  
401 e2020GL088515. doi: 10.1029/2020GL088515
- 402 Jeevanjee, N., & Romps, D. M. (2013). Convective self-aggregation, cold pools, and  
403 domain size. *Geophysical Research Letters*, *40*(5), 994–998. doi: 10.1002/grl  
404 .50204
- 405 Johnson, R. H., Ciesielski, P. E., & Hart, K. A. (1996, July). Tropical Inversions  
406 near the 0°C Level. *Journal of the Atmospheric Sciences*, *53*(13), 1838–1855.  
407 doi: 10.1175/1520-0469(1996)053<1838:TINTL>2.0.CO;2
- 408 Johnson, R. H., Rickenbach, T. M., Rutledge, S. A., Ciesielski, P. E., & Schubert,  
409 W. H. (1999). Trimodal Characteristics of Tropical Convection. *Journal of Cli-*  
410 *mate*, *12*(8), 2397–2418. doi: 10.1175/1520-0442(1999)012<2397:tcotc>2.0.co;2
- 411 Karam, D. B., Flamant, C., Knippertz, P., Reitebuch, O., Pelon, J., Chong, M.,  
412 & Dabas, A. (2008). Dust emissions over the Sahel associated with the  
413 West African monsoon intertropical discontinuity region: A representative  
414 case-study. *Quarterly Journal of the Royal Meteorological Society*, *134*(632),  
415 621–634. doi: 10.1002/qj.244
- 416 Kelly, M. A., & Randall, D. A. (2001). A Two-Box Model of a Zonal Atmospheric  
417 Circulation in the Tropics. *Journal of Climate*, *14*(19), 3944–3964. doi: 10  
418 .1175/1520-0442(2001)014<3944:atbmoa>2.0.co;2
- 419 Kiladis, G. N., Thorncroft, C. D., & Hall, N. M. J. (2006, September). Three-  
420 Dimensional Structure and Dynamics of African Easterly Waves. Part I:  
421 Observations. *Journal of the Atmospheric Sciences*, *63*(9), 2212–2230. doi:  
422 10.1175/JAS3741.1
- 423 Lang, T., Naumann, A. K., Stevens, B., & Buehler, S. A. (2021). Tropical Free-  
424 Tropospheric Humidity Differences and Their Effect on the Clear-Sky Ra-  
425 diation Budget in Global Storm-Resolving Models. *Journal of Advances in*  
426 *Modeling Earth Systems*, *13*(11). doi: 10.1029/2021ms002514
- 427 Larson, K., Hartmann, D. L., & Klein, S. A. (1999). The Role of Clouds, Wa-  
428 ter Vapor, Circulation, and Boundary Layer Structure in the Sensitiv-  
429 ity of the Tropical Climate. *Journal of Climate*, *12*(8), 2359–2374. doi:  
430 10.1175/1520-0442(1999)012
- 431 Lavaysse, C., Flamant, C., Janicot, S., Parker, D. J., Lafore, J.-P., Sultan, B., &  
432 Pelon, J. (2009, August). Seasonal evolution of the West African heat  
433 low: A climatological perspective. *Climate Dynamics*, *33*(2), 313–330. doi:  
434 10.1007/s00382-009-0553-4
- 435 Marsham, J. H., Dixon, N. S., Garcia-Carreras, L., Lister, G. M. S., Parker, D. J.,  
436 Knippertz, P., & Birch, C. E. (2013). The role of moist convection in the  
437 West African monsoon system: Insights from continental-scale convection-  
438 permitting simulations. *Geophysical Research Letters*, *40*(9), 1843–1849. doi:  
439 10.1002/grl.50347
- 440 Mekonnen, A., & Rossow, W. B. (2011). The Interaction Between Deep Convection  
441 and Easterly Waves over Tropical North Africa: A Weather State Perspective.  
442 *Journal of Climate*, *24*(16), 4276–4294. doi: 10.1175/2011jcli3900.1
- 443 Miller, R. L. (1997). Tropical Thermostats and Low Cloud Cover. *Journal of Cli-*  
444 *mate*, *10*(3), 409–440. doi: 10.1175/1520-0442(1997)010<0409:ttalcc>2.0.co;2
- 445 Muller, C., & Bony, S. (2015). What favors convective aggregation and why? *Geo-*  
446 *physical Research Letters*, *42*(13), 5626–5634. doi: 10.1002/2015gl064260
- 447 Muller, C., Yang, D., Craig, G., Cronin, T., Fildier, B., Haerter, J. O., ... Sher-  
448 wood, S. C. (2022). Spontaneous Aggregation of Convective Storms. *Annual*  
449 *Review of Fluid Mechanics*, *54*(1), 133–157. doi: 10.1146/annurev-fluid-022421  
450 -011319
- 451 Muller, C. J., & Held, I. M. (2012). Detailed Investigation of the Self-Aggregation

- of Convection in Cloud-Resolving Simulations. *Journal of the Atmospheric Sciences*, 69(8), 2551–2565. doi: 10.1175/jas-d-11-0257.1
- Parker, D. J., Thorncroft, C. D., Burton, R. R., & Diongue-Niang, A. (2005). Analysis of the African easterly jet, using aircraft observations from the JET2000 experiment. *Quarterly Journal of the Royal Meteorological Society*, 131(608), 1461–1482. doi: 10.1256/qj.03.189
- Peixoto, A. H. O., Jose P. (1992). *Physics of Climate* (1st ed.). American Institute of Physics Melville, NY.
- Pierrehumbert, R. T. (1995). Thermostats, Radiator Fins, and the Local Runaway Greenhouse. *Journal of the Atmospheric Sciences*, 52(10), 1784–1806. doi: 10.1175/1520-0469(1995)052
- Pierrehumbert, R. T. (1998). Lateral mixing as a source of subtropical water vapor. *Geophysical Research Letters*, 25(2), 151–154. doi: 10.1029/97GL03563
- Prange, M., Brath, M., & Buehler, S. A. (2021). Are elevated moist layers a blind spot for hyperspectral infrared sounders? A model study. *Atmospheric Measurement Techniques*, 14(11), 7025–7044. doi: 10.5194/amt-14-7025-2021
- Prange, M., Buehler, S. A., & Brath, M. (2023). How adequately are elevated moist layers represented in reanalysis and satellite observations? *Atmospheric Chemistry and Physics*, 23(1), 725–741. doi: 10.5194/acp-23-725-2023
- Prange, M., Stevens, B., & Buehler, S. A. (2024). *Supplementary data for "Emergence and circulation coupling of moist layers over the tropical Atlantic"*. Zenodo [Dataset, Software]. doi: 10.5281/zenodo.10667051
- Romps, D. M. (2014). An Analytical Model for Tropical Relative Humidity. *Journal of Climate*, 27(19), 7432–7449. doi: 10.1175/jcli-d-14-00255.1
- Schulz, H., & Stevens, B. (2018). Observing the Tropical Atmosphere in Moisture Space. *Journal of the Atmospheric Sciences*, 75(10), 3313–3330. doi: 10.1175/jas-d-17-0375.1
- Sokol, A. B., & Hartmann, D. L. (2022). Congestus Mode Invigoration by Convective Aggregation in Simulations of Radiative-Convective Equilibrium. *Journal of Advances in Modeling Earth Systems*, 14(7), e2022MS003045. doi: 10.1029/2022MS003045
- Stein, T. H. M., Parker, D. J., Delanoë, J., Dixon, N. S., Hogan, R. J., Knipertz, P., ... Marsham, J. H. (2011). The vertical cloud structure of the West African monsoon: A 4 year climatology using CloudSat and CALIPSO. *Journal of Geophysical Research: Atmospheres*, 116(D22). doi: 10.1029/2011JD016029
- Stevens, B. (2017, June). Clouds unfazed by haze. *Nature*, 546(7659), 483–484. doi: 10.1038/546483a
- Stevens, B., & Bony, S. (2013). What Are Climate Models Missing? *Science*, 340(6136), 1053–1054. doi: 10.1126/science.1237554
- Stevens, B., & Brenguier, J.-L. (2009, February). Cloud-controlling Factors: Low Clouds. In J. Heintzenberg & R. J. Charlson (Eds.), *Clouds in the Perturbed Climate System: Their Relationship to Energy Balance, Atmospheric Dynamics, and Precipitation* (p. 0). The MIT Press. doi: 10.7551/mitpress/9780262012874.003.0008
- Stevens, B., Lenschow, D. H., Faloona, I., Moeng, C.-H., Lilly, D. K., Blomquist, B., ... Thornton, D. (2003). On entrainment rates in nocturnal marine stratocumulus. *Quarterly Journal of the Royal Meteorological Society*, 129(595), 3469–3493. doi: 10.1256/qj.02.202
- Stevens, B., Satoh, M., Auger, L., Biercamp, J., Bretherton, C. S., Chen, X., ... Zhou, L. (2019). DYAMOND: The DYNAMics of the Atmospheric general circulation Modeled On Non-hydrostatic Domains. *Progress in Earth and Planetary Science*, 6(1), 61. doi: 10.1186/s40645-019-0304-z
- Thorncroft, C., & Hodges, K. (2001, March). African Easterly Wave Variability and Its Relationship to Atlantic Tropical Cyclone Activity. *Journal of Climate*,

- 507           14(6), 1166–1179. doi: 10.1175/1520-0442(2001)014(1166:AEWVAI)2.0.CO;2  
508   Trenberth, K. E., Stepaniak, D. P., & Caron, J. M. (2000, November). The Global  
509   Monsoon as Seen through the Divergent Atmospheric Circulation. *Journal of*  
510   *Climate*, 13(22), 3969–3993. doi: 10.1175/1520-0442(2000)013(3969:TGMAS)  
511   2.0.CO;2
- 512   Villiger, L., Wernli, H., Boettcher, M., Hagen, M., & Aemisegger, F. (2022). La-  
513   grangian formation pathways of moist anomalies in the trade-wind region dur-  
514   ing the dry season: Two case studies from EUREC4A. *Weather and Climate*  
515   *Dynamics*, 3(1), 59–88. doi: 10.5194/wcd-3-59-2022
- 516   Wing, A. A., Emanuel, K., Holloway, C. E., & Muller, C. (2017). Convective Self-  
517   Aggregation in Numerical Simulations: A Review. *Surveys in Geophysics*,  
518   38(6), 1173–1197. doi: 10.1007/s10712-017-9408-4
- 519   Wing, A. A., Reed, K. A., Satoh, M., Stevens, B., Bony, S., & Ohno, T. (2018).  
520   Radiative–convective equilibrium model intercomparison project. *Geoscientific*  
521   *Model Development*, 11(2), 793–813. doi: 10.5194/gmd-11-793-2018